



**HAL**  
open science

# A new estimation of equivalent matrix block sizes in fractured media with two-phase flow applications in dual porosity models

Chahir Jerbi, André Fournon, Benoit Noetinger, Frédérick Delay

## ► To cite this version:

Chahir Jerbi, André Fournon, Benoit Noetinger, Frédérick Delay. A new estimation of equivalent matrix block sizes in fractured media with two-phase flow applications in dual porosity models. *Journal of Hydrology*, 2017, 548, pp.508-523. 10.1016/j.jhydrol.2017.03.028 . hal-01738345

**HAL Id: hal-01738345**

**<https://ifp.hal.science/hal-01738345>**

Submitted on 20 Mar 2018

**HAL** is a multi-disciplinary open access archive for the deposit and dissemination of scientific research documents, whether they are published or not. The documents may come from teaching and research institutions in France or abroad, or from public or private research centers.

L'archive ouverte pluridisciplinaire **HAL**, est destinée au dépôt et à la diffusion de documents scientifiques de niveau recherche, publiés ou non, émanant des établissements d'enseignement et de recherche français ou étrangers, des laboratoires publics ou privés.

1 **A new estimation of equivalent matrix block sizes in fractured media with two-phase**  
2 **flow applications in dual porosity models**

3 Chahir Jerbi<sup>1</sup>, André Fournon<sup>1</sup>, Benoit Noetinger<sup>1</sup>, Frederick Delay<sup>2\*</sup>

4  
5 <sup>1</sup> IFP Energies Nouvelles, 1&4 Avenue du Bois Préau 92500 Rueil-Malmaison, France.

6 <sup>2</sup> Laboratoire d'Hydrologie et de Géochimie de Strasbourg, Univ. Strasbourg/EOST, CNRS  
7 UMR 7517, 1 rue Blessig, 67000 Strasbourg, France

8 \* Corresponding author: Phone +33 3 68 85 04 16; Fax +33 3 68 85 04 02; mail fdelay@unistra.fr

9  
10 **Abstract**

11 Single and multiphase flows in fractured porous media at the scale of natural  
12 reservoirs are often handled by resorting to homogenized models that avoid the heavy  
13 computations associated with a complete discretization of both fractures and matrix blocks.  
14 For example, the two overlapping continua (fractures and matrix) of a dual porosity system  
15 are coupled by way of fluid flux exchanges that deeply condition flow at the large scale. This  
16 characteristic is a key to realistic flow simulations, especially for multiphase flow as capillary  
17 forces and contrasts of fluid mobility compete in the extraction of a fluid from a capacitive  
18 matrix then conveyed through the fractures. The exchange rate between fractures and matrix  
19 is conditioned by the so-called mean matrix block size which can be viewed as the size of a  
20 single matrix block neighboring a single fracture within a mesh of a dual porosity model.

21 We propose a new evaluation of this matrix block size based on the analysis of  
22 discrete fracture networks. The fundamentals rely upon establishing at the scale of a fractured  
23 block the equivalence between the actual fracture network and a Warren and Root network  
24 only made of three regularly spaced fracture families parallel to the facets of the fractured  
25 block. The resulting matrix block sizes are then compared via geometrical considerations and

26 two-phase flow simulations to the few other available methods. It is shown that the new  
27 method is stable in the sense it provides accurate sizes irrespective of the type of fracture  
28 network investigated. The method also results in two-phase flow simulations from dual  
29 porosity models very close to that from references calculated in finely discretized networks.  
30 Finally, calculations of matrix block sizes by this new technique reveal very rapid, which  
31 opens the way to cumbersome applications such as preconditioning a dual porosity approach  
32 applied to regional fractured reservoirs.

33

34 **Keywords**

35 Fractured porous media; Matrix block sizes; Dual porosity models; Multiphase flow.

36 **1. Introduction**

37           Conventional oil reservoirs are often housed in fractured rocks, especially in  
38 carbonates environments, and one can estimate that more than 30 % of world oil reserves are  
39 concealed in densely fractured systems, oil being mainly trapped in the host rock matrix.  
40 Paradoxically, these geological structures may trigger contrasted effects on large-scale two-  
41 phase flow patterns by increasing oil recovery due to high local permeability values, or on the  
42 opposite, by decreasing oil extraction rates because of early water invasion, viscous fingering  
43 etc. The same type of behavior is also encountered in the context of water decontamination  
44 and can become even more complex if oil (and/or water) is swept by injections of miscible  
45 gas.

46           Modeling two-phase flow in fractured reservoirs is now often employed for the  
47 purpose of various applications, for instance to assess the relevance of different oil recovery  
48 strategies or to investigate on the feasibility of in-situ water decontamination processes  
49 (Bourbiaux, 2010). This fact makes that modeling single phase or multiphase flow in  
50 fractured media is still a fertile research domain even though pioneering works on the topic  
51 started in the early sixties (e.g., in Lemonnier et al., 2010a, b).

52           In this context, flow simulations relying upon finely gridded discrete fracture networks  
53 and their associated (discretized) matrix blocks are becoming increasingly popular because of  
54 the availability of high performance computers, the progress in algorithms for meshing  
55 complex geometries, and the availability of sophisticated numerical techniques for solving  
56 partial differential equations (Landereau et al., 2001; Noetinger et al., 2001; Adler et al.,  
57 2005; Matthäi and Nick, 2009; Fournon et al., 2013). This exhaustive approach is critical to  
58 bring us reference solutions and various benchmarks with which simpler approaches can be  
59 compared. Nevertheless, gridded discrete fracture networks may be poorly documented and  
60 include flawed information in the case of real-world applications. In addition, finely gridded

61 systems remain hardly usable for current practical applications to large-scale systems that  
62 result in cumbersome model parameterizations and heavy computations. This downside is  
63 emphasized in the domain of petroleum engineering usually dealing with both non-linear  
64 multiphase flow and dense fracture networks requiring huge discretization efforts (Landereau  
65 et al., 2001; Adler et al., 2005; Fournon et al., 2013). Applicability is also hindered by  
66 duplicated calculations if the study encompasses tests of various model designs, various  
67 model parameterization and various flow scenarios.

68         Fortunately, dense fracture networks are also good candidates to homogenization at  
69 the scale of reasonable elementary mesh sizes (on the order of 5-100 m) by resorting for  
70 example to the dual porosity approach to fractured media initially developed by Barenblatt et  
71 al. (1960). The dual porosity formulation conceptualizes a fractured system as two  
72 overlapping continua merging a fracture medium and a matrix medium with contrasts of  
73 hydraulic properties between the two continua. Flow is then described by a set of equations in  
74 each continuum (this set depends on the type of flow and the fluid phases present in the  
75 system) associated with an exchange term ruling the fluid fluxes percolating between  
76 continua.

77         This exchange term is all the more important that in general fractures are conveying  
78 flow as the matrix stores fluid volumes. In transient problems as for example forced flow  
79 between injecting and extracting wells, the way the relationship establishes between storage  
80 capacity and conduction property conditions the overall response of the reservoir (e.g., Acuna  
81 and Yortsos, 1995). In the specific cases of two-phase flow (water and oil), the absence or the  
82 weak incidence of capillary forces in open fractures makes that flow is locally mainly of  
83 single-phase type conveying either oil or water (with sharp saturation fronts in between) at  
84 different locations in the fracture network. For its part, the way the matrix blocks are soaked  
85 (water invades the matrix and pushes oil away) or drained (oil pushes water) strongly depends

86 on matrix block sizes and on the petro-physics properties of the matrix, making that extraction  
87 from the matrix of a fluid by the other is mainly driven by capillary forces or by capillary  
88 forces plus viscous forces (single-phase Darcian flow to make it simple).

89         When a discrete fracture network is connected enough and handled at an elementary  
90 scale larger than a representative elementary volume, the exchange term in the dual porosity  
91 models is proportional to an equivalent matrix block size. Intuitively, a REV for a fracture  
92 network is a volume within which mean properties of the network such as fracture density,  
93 fracture aperture, fracture hydraulic conductivity have some statistical meaning (Long et al.,  
94 1982; Neuman, 1988). In a dual porosity model, the REV is also associated with the  
95 capability to represent the actual fracture network as a synthetic network made (in three-  
96 dimensional problems) of three regularly spaced fracture families, each family developing  
97 fracture planes normal to one of the three main directions of flow. The so-called DFN  
98 homogenized as a "sugar-cube" model (Warren and Root, 1963) is at the origin of the notion  
99 of the equivalent matrix block size in relation with the dimensions of the elementary "sugar  
100 piece" separating neighbor fractures in the homogenized DFN (Kazemi et al., 1976).

101         There exist two types of methods to evaluate the elementary matrix block size. The  
102 first type relies upon exercises matching actual well test drawdown curves with analytical  
103 solutions that inherit from rigorous mathematical homogenization or large-scale averaging  
104 techniques (Arbogast 1990; Quintard and Whitaker, 1993; Noetinger et al., 2001; Unsal et al.,  
105 2010; Noetinger and Jarrige, 2012). The downside of these techniques is that sometimes  
106 actual well testing in fractured rock do not exist and when these tests exist, the damaged zone  
107 in the close vicinity of a well may not fully reflect flow conditions in the natural fracture  
108 network. The second type of methods is based on geometrical considerations regarding the  
109 fracture network. These considerations led to three geometrical approaches that are the  
110 geometrical imbibition method (GI, Bourbiaux et al., 1997), the enhanced general imbibition

111 method (EGI, Bourbiaux et al., 2006), and the mean spacing method (MS, Narr, 1996). It is  
112 obvious that these approaches can only be applied if a minimum prior knowledge about the  
113 fracture network geometry is available.

114 In this contribution we propose a new geometrical method that can to some extent  
115 overlook the actual geometry of the fracture network because the method relies upon the  
116 identification of a sugar-cube DFN equivalent to the actual network (see details hereafter).  
117 The method also allows us to calculate matrix block sizes along directions parallel to the main  
118 flow directions that are conditioned by the geometry of the fracture network (or its equivalent  
119 as a sugar-cube model). Section 2 (and Appendix A) is focused on the theoretical framework  
120 we rely upon to build the so-called oriented block size (OBS) method that we propose. For the  
121 sake of clarity, a few features about dual-porosity models are also reminded. The matrix block  
122 sizes stemming from the OBS technique are then compared to that from the other geometrical  
123 techniques (GI, EGI, and MS, see above). The comparison is performed by way of a suite of  
124 calculations applied to synthetic random fracture networks for which we explicitly control  
125 both the geometric and hydraulic properties of the networks and the mean size of matrix  
126 blocks between fractures. As told earlier, only dense and well-connected fracture networks are  
127 considered because sparse networks cannot be homogenized via a dual porosity model at the  
128 scale of a complete underground reservoir. Section 4 evaluates the OBS technique and also  
129 the other geometrical approaches within the framework of a dual-porosity model compared  
130 with exhaustive calculations discretizing the fracture network and the matrix blocks. The two-  
131 phase flow scenarios are either dominated by capillary forces or viscous forces in an exercise  
132 which consists in draining oil from matrix blocks by injecting water in fractures. These  
133 complex flow scenarios are performed over synthetic test cases in which we control the  
134 reference calculations (in a fully discretized system). This procedure enable us to clearly

135 emphasizes the main theoretical findings regarding matrix block size in dual porosity models  
 136 before envisioning further concrete field-scale applications.

137

## 138 **2. Theoretical background**

139 In various approaches to fractured systems, the duality of fracture networks embedded  
 140 in a host rock matrix is often represented as two overlapping continua merging a fracture  
 141 medium and a matrix medium. In a so-called dual porosity – single permeability model, the  
 142 fractures are usually highly conductive and poorly capacitive as the matrix is highly  
 143 capacitive but with negligible flow triggered by fluid pressure gradients (weak permeability).  
 144 As an example, single-phase Darcian flow in a dual continuum approach results in the  
 145 resolution of two equations in the form

$$146 \quad \frac{\partial(\rho\phi^f)}{\partial t} + \nabla \cdot \left( -\rho \frac{\mathbf{k}^f}{\mu} \cdot \nabla (P^f + \rho g z) \right) - E^{m \rightarrow f} = 0 \quad (1)$$

$$147 \quad \frac{\partial(\rho\phi^m)}{\partial t} + E_p^{m \rightarrow f} = 0 \quad ; \quad E_p^{m \rightarrow f} = \rho \sigma \frac{\mathbf{k}^m}{\mu} (P^m - P^f) \quad (2)$$

148 For the sake of simplicity, references to space (x) and time (t) for parameters and state  
 149 variables have been dropped. The indexes f and m refer to fracture and matrix continua,  
 150 respectively.  $\rho$  [ML-3] is the mass density of the fluid,  $\mu$  [ML-1T-1] is the dynamic  
 151 viscosity of the fluid,  $\mathbf{k}^\lambda$  [L2] is the permeability of the continuum  $\lambda$  ( $\lambda = f, m$ ),  $\phi^\lambda$  [-] is  
 152 the porosity of the continuum  $\lambda$ ,  $P^\lambda$  [ML-1T-2] is the fluid pressure in the continuum  $\lambda$ ,  $g$   
 153 [LT-2] is the scalar value of the gravity acceleration  $g$ , and  $z$  [L] is the local elevation taken  
 154 from an arbitrary reference and counted positive upward.  $E_p^{m \rightarrow f}$  [ML<sup>-3</sup>T<sup>-1</sup>] is the exchange  
 155 rate (a mass fluid flux per unit volume of medium) between the fracture and the matrix  
 156 continua.



157 In (2), the exchange rate is of pseudo steady-state type meaning that the relationship  
158 between matrix and fractures depends on pressure gaps between the continua and not on a  
159 convolution product of their derivatives with respect to time. In (2), the matrix permeability  
160  $\mathbf{k}^m$  is assumed small enough to neglect Darcian fluxes in the matrix (compared to that in the  
161 fractures) but large enough to enable fluid flux percolation between the matrix and the  
162 fractures. Therefore, the matrix permeability is an entry of the exchange rate via the term  
163  $\sigma \mathbf{k}^m$ ,  $\sigma$  [ $L^{-2}$ ] being a shape factor tensor that quantifies the mean size of the matrix blocks  
164 associated with the fractures included in an elementary volume (for example, the volume  
165 corresponding to the elementary meshing employed when solving numerically Eqs (1) and  
166 (2)). By construction, the pseudo steady-state assumption in (2) ignores the early transient  
167 flow regime between matrix and fractures which may result in erroneous evaluations of  
168 exchanged fluid fluxes, especially in the case of weakly permeable matrix media requiring  
169 long times for equilibrating their fluid pressure fields with that of fractures (e.g., as in shale  
170 gas and shale oil extraction problems). Transient exchange rates between fractures and matrix  
171 are the natural outcome of Multiple INteracting Continua (MINC approaches) initially  
172 developed in the late eighties (e.g., Pruess and Narasimhan, 1985; Pruess et al., 1990) and  
173 more recently reassessed and improved (e.g., Karimi-Fard et al., 2006; Tatomir et al., 2011,  
174 de Dreuzy et al., 2013). The MINC models are not incompatible with the notion of mean  
175 matrix block size in homogenized fractured systems as each matrix block is viewed as an  
176 entity of prescribed size enclosing a nested heterogeneity.

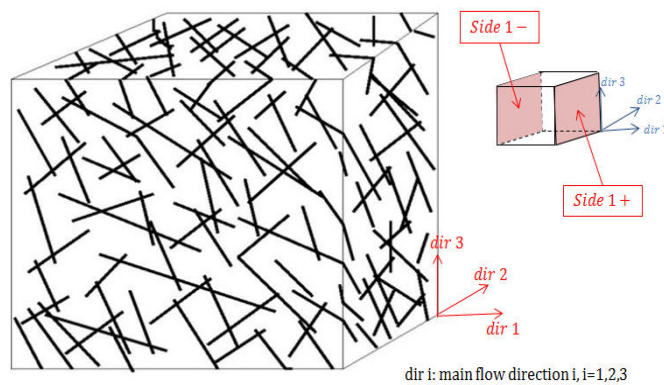
177 Various formulations of the shape factor have been proposed for many modeling  
178 applications (Kazemi et al., 1976; Thomas et al., 1983; Coats 1989; Ueda et al., 1989; Lim et  
179 al. 1995; Quintard and Whitaker, 1996; Noetinger and Estebenet., 2000) amongst which the  
180 formulation proposed by Kazemi et al. (1976) is the one used in this study. This choice is  
181 motivated by a quite simple formulation which allows for dealing with diagonal tensors, and

182 also introduces the mean matrix block size as a quantity weighting the influence of the matrix  
 183 permeability tensor to control the fluid fluxes exchanges between matrix and fractures. For  
 184 diagonal permeability and shape factor tensors, the product  $\sigma \mathbf{k}^m$  is developed as

$$185 \quad \sigma \mathbf{k}^m = \begin{pmatrix} k_x^m / s_x^2 & 0 & 0 \\ 0 & k_y^m / s_y^2 & 0 \\ 0 & 0 & k_z^m / s_z^2 \end{pmatrix} \quad (3)$$

186 with  $s_i$  [L] ( $i=x, y, z$ ) the mean matrix block size along the main flow direction  $i$ . As the  
 187 exchange rate between the fractures and the matrix is a key feature to the behavior of a dual  
 188 continuum and some other homogenized approaches (Lemonnier et al., 2010a, b), it makes  
 189 sense to revisit the item especially regarding the mean matrix block size (which rules the  
 190 fluxes, provided the fluid pressure fields are correctly calculated).

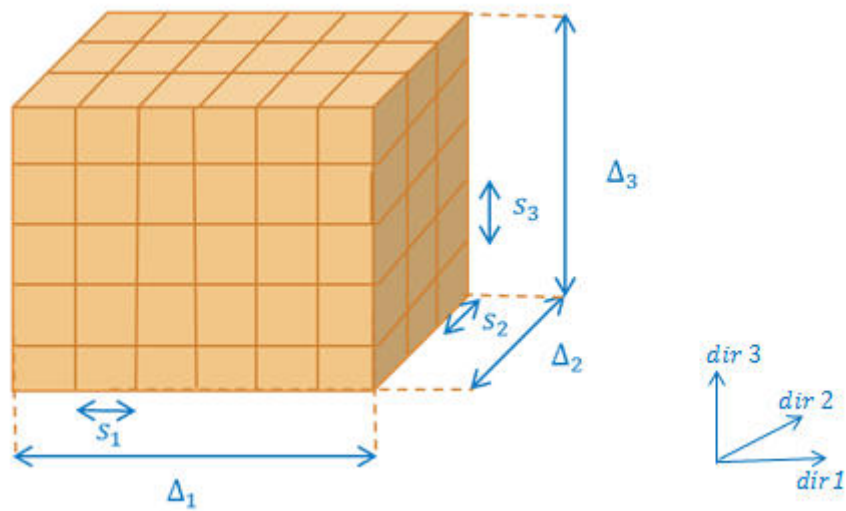
191 The Oriented Block Size (OBS) technique that we develop below infers the mean  
 192 matrix blocks sizes  $s_i$  ( $i=x, y, z$ ) from a fractured system by assuming that a rock block  
 193 enclosing an actual fracture network with various characteristics (e.g., Fig 1) can be turned  
 194 into a simplified block with an equivalent fracture network composed of three families of  
 195 planar fractures.



196  
 197 Fig. 1. A fractured rock block at the scale of a reservoir grid cell with references to main flow  
 198 directions and facets of block normal to flow directions.

199

200 Each family is defined by a uniform spacing between fractures and a fracture plane normal to  
 201 one direction of flow (or including the two other directions). This equivalent fracture network  
 202 (e.g., Fig. 2) which draws the so-called "sugar-cube" configuration as proposed by Warren  
 203 and Root (1963) and referred to as the WR model hereafter, is conceptually compatible with  
 204 the notion of mean matrix block size. The three families of WR fractures delimit a  
 205 parallelepiped elementary block separating neighbor fractures that should coincide with the  
 206 shape factor as defined in Eq (3). If the whole WR block is wide enough, the three fracture  
 207 families can be aggregated as a single fracture permeability tensor (or value) and a single  
 208 fracture porosity for the whole block or its facets. These parameters depend on the size of the  
 209 elementary matrix block separating the WR fractures. By comparing, or more exactly by  
 210 identifying permeability and porosity properties of a WR block with that of an actual  
 211 fractured block, one is able to define the equivalent mean matrix block size of the actual  
 212 fractured block.



213  
 214 Fig. 2. A regular fracture network of three fracture families (a Warren and Root (WR) model)  
 215 at the scale of a reservoir grid cell with reference to main flow directions, facets of block  
 216 normal to flow directions, and spacing between fractures.

217

218

219 Let us take a parallelepiped block housing an actual fracture network as depicted in  
220 Fig. 1. The first way to identify a single macroscopic permeability tensor  $\mathbf{k}^f$  for the block is  
221 to employ upscaling approaches, multiple continua theory (Karimi-Fard et al., 2006; Tatomir  
222 et al., 2011; Jourdain et al., 2014), analytical solutions (Oda, 1985) or simply to conjecture the  
223 entries of the tensor as could be done, for example, in parameterizing a dual porosity approach  
224 after having postulated that the approach was convenient for the problem under investigation.  
225 A second way is to extract the (diagonal) tensor from the structural properties of the fracture  
226 network and its relationships with the homogenization volume (the block) concealing it.

227 The actual fractured block as depicted in Fig 1 is oriented with its main directions  
228 along the main directions of flow indexed by  $i=1,2,3$  (here completely equivalent to  $i = x, y, z$   
229 for locations in space denoted  $\mathbf{x} = (x, y, z)$  but easier to manipulate when incrementing the  
230 index). The block size in direction  $i$  is denoted  $\Delta_i$  and the sides delimiting the block are also  
231 indexed by  $i$  but for limits normal to the main direction  $i$ . In addition, block sides are labelled  
232  $i^-$  or  $i^+$  according to their respective location upstream or downstream along direction  $i$ .  
233 Assuming that the fractured block is well connected, the mean permeability of the block along  
234 a direction  $i$  can be calculated as the average over the sides  $i^-$  and  $i^+$  of the local  
235 permeability of fractures intercepting the sides. This yields

$$236 \quad k_i^{FN-S} = \frac{1}{2(\Delta_{i+1}\Delta_{i+2})} \left( \sum_{n=1}^{Nf_{i-}} k_n l_n e_n + \sum_{n=1}^{Nf_{i+}} k_n l_n e_n \right) \quad (4)$$

237 In the above equation,  $i$  is a cycling index such that, e.g.,  $i+1 = 3$  when  $i = 2$  and  $i+1$  returns  
238 to 1 when  $i=3$ .  $k_i^{FN-S}$  [ $L^2$ ] is the macroscopic fracture permeability of the fractured block  
239 along direction  $i$ ,  $\Delta_{i+1}\Delta_{i+2}$  [ $L^2$ ] is the total surface area of sides  $i^-$  and  $i^+$  these being  
240 intercepted by a number of fractures  $Nf_{i-}$  and  $Nf_{i+}$ .  $k$  [ $L^2$ ] is the local permeability of a

241 fracture seen as intercepting the side of the block over an apparent length  $l$  and with apparent  
 242 fracture aperture  $e$  [L].

243 By re-using the same notations for directions and sides in a rock block modeled as a  
 244 WR network (Fig. 2), one can also calculate the entries  $k_i^{WR}$  of the diagonal fracture  
 245 permeability tensor of the WR block along directions  $i$ . The three fracture families of the WR  
 246 network are also indexed by  $i$  with the same notation as for the block sides, i.e., a fracture  
 247 family  $i$  corresponds to fracture planes normal to direction  $i$ . A family  $i$  is of uniform spacing  
 248  $s_i$  [L] ( $s_i$  is measured along direction  $i$ , see Fig. 2), counts  $Nf_i$  fractures with a uniform  
 249 scalar permeability  $k_i$  and a uniform fracture aperture  $e_i$ . With these settings and the  
 250 assumption that flow only occurs in the fractures, the total flow rate entering or exiting the  
 251 WR fractured block through a side  $i$  normal to the direction  $i$  can be expressed as

$$252 \quad Q_i = -\nabla_i P \left( \sum_{j \neq i} Nf_j e_j \Delta_{k;k \neq i, k \neq j} \frac{k_j}{\mu} \right) = -\nabla_i P \frac{k_i^{WR}}{\mu} \Delta_{i+1} \Delta_{i+2} \quad (5)$$

253 For the sake of simplicity, the gravity components of flow have not been accounted for in (5).  
 254  $Nf_j e_j \Delta_{k;k \neq i, k \neq j}$  represents the total surface of flow developed by the family fracture  $j$  through  
 255 the side  $i$  of the block,  $\Delta_{i+1} \Delta_{i+2}$  is the total surface area of the side  $i$ , and  $k_i^{WR}$  is the  
 256 macroscopic fracture permeability of the WR block along direction  $i$ . The equality in (5)  
 257 comes down to a direct identification of the three terms of the macroscopic permeability  $\mathbf{k}^{WR}$   
 258 as

$$259 \quad \begin{bmatrix} k_1^{WR} \\ k_2^{WR} \\ k_3^{WR} \end{bmatrix} = \begin{bmatrix} 0 & 1/\Delta_2 & 1/\Delta_3 \\ 1/\Delta_1 & 0 & 1/\Delta_3 \\ 1/\Delta_1 & 1/\Delta_2 & 0 \end{bmatrix} \cdot \begin{bmatrix} Nf_1 e_1 k_1 \\ Nf_2 e_2 k_2 \\ Nf_3 e_3 k_3 \end{bmatrix} \quad (6)$$

260 In the context of scaling the values  $k_i^{WR}$  so they become equivalent to calculated values in a  
 261 rock block encapsulating an actual fracture network, the number  $Nf_i$  of WR fractures, their

262 aperture  $e_i$  and their permeability  $k_i$  become the unknowns of the problem. Therefore, it  
 263 makes sense to invert the linear system of equation (6) which yields

$$264 \quad Nf_i e_i k_i = \frac{\Delta_i}{2} \sum_{j=1}^3 (-1)^{\delta_{i,j}} k_j^{WR} \quad (7)$$

265 with  $\delta_{i,j}$  the Kronecker delta function,  $\delta_{i,j} = 1$  if  $i = j$  and  $\delta_{i,j} = 0$  if  $i \neq j$ .

266 By considering the structure of a WR fracture network, one can write

$$267 \quad Nf_i (e_i + s_i) = \Delta_i \Rightarrow \frac{Nf_i e_i}{\Delta_i} = \frac{e_i}{e_i + s_i} \quad (8)$$

268 Note in the above expression that counting  $Nf_i$  fractures assumes the presence of  $Nf_i - 1$   
 269 fractures inside the block and that the two sides  $i$  of the block are each bounded by half a  
 270 fracture of family  $i$  with half the aperture  $e_i$  counted in the block. Introducing (8) in (7)  
 271 results in

$$272 \quad k_i = \frac{1}{2} \left( 1 + \frac{s_i}{e_i} \right) \sum_{j=1}^3 (-1)^{\delta_{i,j}} k_j^{WR} \quad (9)$$

273 The expression (9) will be used later for the purpose of identification between an actual  
 274 fractured block and a WR block.

275 Let us look at the porosity properties of the WR block. The fracture porosity  $\phi^{WR}$  [-] of  
 276 the whole WR block and the fracture density  $\phi_i^{WR-S}$  [-] at a side  $i$  defined as the porosity of  
 277 fracture network at a side of the block (the ratio of the surface area of open fractures at a side  
 278 to the total surface of the side) can also be derived as

$$279 \quad \phi^{WR} \approx \sum_{i=1}^3 \frac{Nf_i e_i \Delta_{i+1} \Delta_{i+2}}{\Delta_1 \Delta_2 \Delta_3} = \sum_{i=1}^3 \frac{Nf_i e_i}{\Delta_i} \quad (10)$$

$$280 \quad \phi_i^{WR-S} \approx \sum_{l \neq i} \frac{Nf_l e_l}{\Delta_l} \quad (11)$$

281 Notably, the expressions in (10) and (11) are rather simple but are approximations since the  
 282 intersections of fractures are counted twice in the porosity values. This was found of  
 283 negligible influence for classical block sizes and fracture apertures. Subtracting (11) from (10)  
 284 returns the term  $Nf_i e_i / \Delta_i$  which also appears in Eq (8). Therefore, another way to express the  
 285 relationship between the local WR fracture permeability  $k_i$  and the macroscopic permeability  
 286  $\mathbf{k}^{WR}$  in (9) is

$$287 \quad k_i = \frac{1}{2(\phi^{WR} - \phi_i^{WR-S})} \sum_{j=1}^3 (-1)^{\delta_{i,j}} k_j^{WR} \quad (12)$$

288 Both expressions (9) and (12) are employed to define the matrix block size  $s_i$  (in 9).

289 If the WR network is equivalent regarding its hydraulic properties to the actual  
 290 fracture network, it is expected that  $\phi^{WR}$ ,  $\phi_i^{WR-S}$ , and  $k_j^{WR}$  are similar to the equivalent  
 291 properties in the actual block of fracture network, respectively denoted as  $\phi^{FN}$ ,  $\phi_i^{FN-S}$ , and  
 292  $k_j^{FN-S}$  (see (4) for the latter term). It is also expected that the WR network, while being still  
 293 equivalent to the actual fractured block, can inherit some properties (parameters) of a  
 294 homogenized model such as the mean matrix block sizes of the medium and the permeability  
 295 tensor at the macroscopic scale of a fractured block. By imposing these properties in (9) and  
 296 (12), and after a few algebraic manipulations (see Appendix A for details), an expression of  
 297 the mean matrix block sizes in a homogenized fractured block can be written as

$$298 \quad s_i \approx \frac{\sum_{j=1}^3 (-1)^{\delta_{i,j}} k_j^{FN-S}}{(\phi^{FN*} - \phi_i^{FN-S*}) \sum_{j=1}^3 (-1)^{\delta_{i,j}} k_j^f} \quad (13)$$

299  $k_i^{FN-S}$  ( $i=1,2,3$ ) are the permeability values at the sides  $i$  of the actual fractured block,  
 300  $k_i^f$  ( $i=1,2,3$ ) are the entries of the diagonal permeability tensor of an homogenized medium  
 301 equivalent to the fractured block (e.g., that of a dual porosity model), and  $\phi^{FN*}$ ,

302  $\phi_i^{FN-S^*}$  ( $i = 1, 2, 3$ ) are rescaled block and side porosities of the actual fractured block. These  
303 rescaled porosities of dimension  $[L^{-1}]$  (a porosity per unit fracture aperture) are calculated  
304 over the skeleton of the actual fracture network to which each fracture is assigned a unit  
305 fracture aperture.

306 In addition to postulating the equivalence between a WR block and the actual fractured  
307 block, the assumptions allowing us to derive (13) are twofold. First, the actual fracture  
308 network is a good candidate for homogenization with the meaning that there exist  
309 macroscopic properties as mean matrix block size and diagonal permeability tensor  
310 characterizing the hydraulic behavior of the network at the large scale (at least, the scale of a  
311 mesh of a homogenized model). Second, a WR network exists (as that investigated by way of  
312 equations 5 to 12) but with uniform fracture aperture  $e_f$  over its three fracture families and  
313 still equivalent to the actual fracture network (see Appendix A for details). There is no clear  
314 criterion (except dealing with a dense and well-connected network) allowing us to state  
315 beforehand whether or not a given fracture network would follow the above assumptions.  
316 Eventual criteria would also depend on the flow processes and mechanisms targeted for  
317 further applications at the large scale.

318 It is worth to note that Eq. (13) depends on both the facet permeability values of the  
319 actual fractured block  $k_j^{FN-S}$ , and the structural properties of the actual fracture network  
320 skeleton in the form of porosities  $\phi^{FN^*}$  and  $\phi_i^{FN-S^*}$ . These features make that applicability of  
321 (13) is conditioned by a good knowledge of the actual fracture network geometry and, as a  
322 downside, renders the method hardly applicable to poorly-known natural systems. In the end,  
323 Eq. (13) should be mainly used in problems dealing with homogenization of systems with  
324 well-known geometry and discretization of synthetic fracture networks (as done for instance  
325 in reservoir engineering when passing from a geological model to a tractable flow model).



326 This notwithstanding, the OBS technique can also deliver another form of the mean  
 327 matrix block size. By manipulating the expression of the side block permeability of the actual  
 328 fractured block in (4), scaling the subsequent expression with the side block porosities  $\phi_i^{FN-S}$   
 329 and making use of (13) (details are provided in Appendix A), another form of the mean matrix  
 330 block size comes up as

$$331 \quad s_i \approx \frac{2e_f \bar{k}}{\sum_{j=1}^3 (-1)^{\delta_{i,j}} k_j^f} \quad (14)$$

332 This form introduces the existence of a mean single fracture aperture  $e_f$  [L] (which is also the  
 333 uniform aperture mentioned above for the WR network) and a mean single-fracture  
 334 permeability  $\bar{k}$  [L<sup>2</sup>] at the scale of the whole actual fractured block. These two quantities are  
 335 additional assumptions to that discussed regarding (13) for the applicability of (14).

336 Even though these assumptions may appear very restrictive, they give the possibility  
 337 to infer mean matrix block sizes from poorly known and hardly accessible fracture networks  
 338 as often encountered in field case applications. The entries  $k_j^f$  of the permeability tensor of  
 339 the whole fractured block can be evaluated by way of hydraulic tests; preferably interference  
 340 testing between distant wells that avoid bias stemming from an environment close to the  
 341 tested well that would not be representative of the fracture network at a larger scale. Values of  
 342 uniform single-fracture aperture  $e_f$  and uniform single-fracture permeability  $\bar{k}$  are harder to  
 343 infer because data obtained for instance from optic imaging of boreholes (for  $e_f$ ) and flow or  
 344 production logs (for  $\bar{k}$ ) may reveal not representative of the whole network. It remains that  
 345 the matrix block size calculation in (14) is feasible without resorting to any knowledge on the  
 346 structure of the actual fracture network. It is obvious that the subsequent inferred value of  
 347 mean matrix block size should be taken as an order of magnitude (then refined for instance by  
 348 model inversion) instead of a robust pinpoint value.

349 In the following comparing: 1- the OBS technique with other geometrical techniques,  
350 and 2- the dual porosity approach (handling matrix block sizes  $s_i$ ) with finely discretized  
351 networks, we address the relevance of the simplified expression in (14) under the assumption  
352 that the skeleton of the fracture network is known (as is the case with other geometrical  
353 methods). We prescribe to each fracture a uniform aperture and a uniform fracture  
354 permeability. The skeleton is then discretized and the entries  $k_j^f$  of the permeability tensor are  
355 calculated by performing numerical "permeameter" experiences (i.e., calculating fluid fluxes  
356 between opposite facets of the fractured block under prescribed Dirichlet boundary conditions  
357 while the other facets of the block are of no-flow type).

358

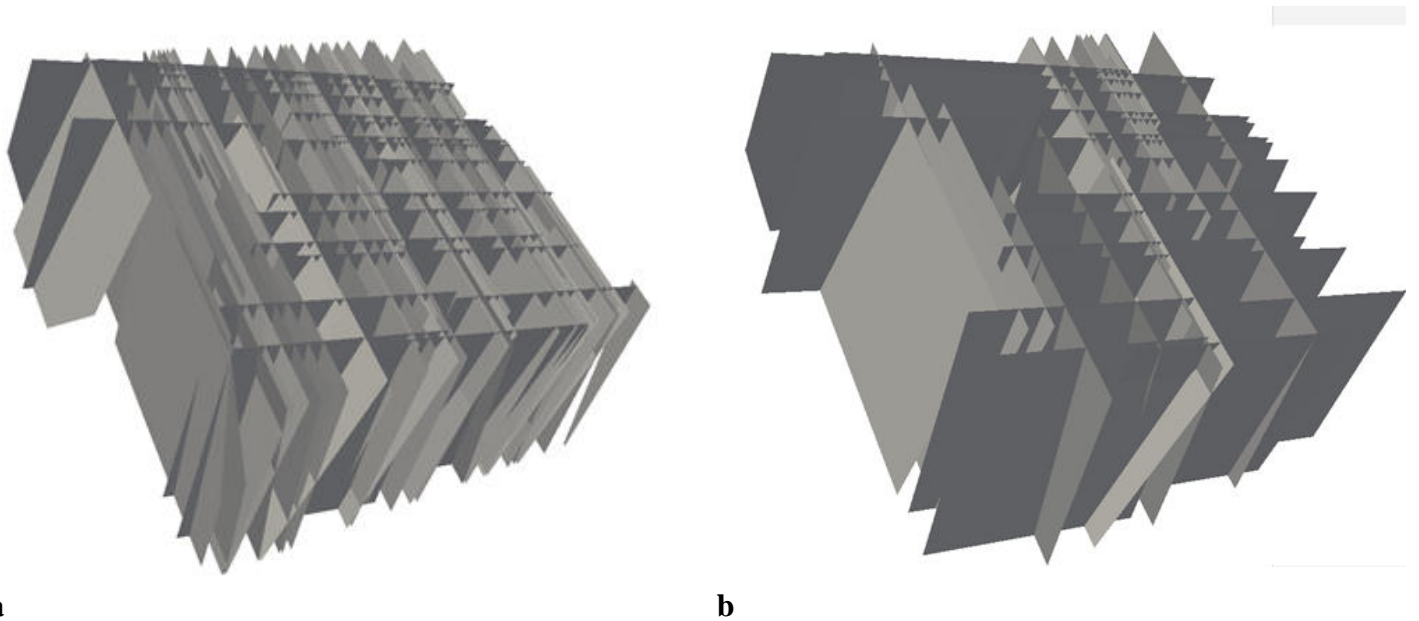
### 359 **3. Comparison with structural-geometrical approaches**

360 As shown from a theoretical standpoint, the OBS technique defines a mean matrix  
361 block size as a measure drawn from geometrical and structural properties of a discrete fracture  
362 network and its equivalent representation via a regular "sugar cube" network. In theory, no  
363 reference to any calculation of flow at the large scale is evoked in obtaining the OBS matrix  
364 block size, which renders the technique comparable in its spirit to other previous approaches  
365 also based on geometrical-structural characteristics of the discrete fracture network.

366 In the following, the OBS evaluation of matrix block sizes is compared with three  
367 other types of geometrical calculations, namely: the geometrical imbibition (GI) technique  
368 (Bourbiaux, 1997), the extended geometrical imbibition (EGI) technique (Bourbiaux et al.,  
369 2006), and the mean spacing (MS) technique (Narr, 1993). The main backgrounds of GI, EGI,  
370 and MS are summarized (sometimes slightly enhanced, as for EGI) and presented with  
371 notations consistent with that of the present work in Appendix B. GI and EGI techniques are  
372 only applicable (in their original version) to two-dimensional fracture networks and model the  
373 distance between any location in the matrix and the nearest fracture of the DFN. MS is

374 available for two- and three-dimensional systems and infers the mean lag distance between  
375 two neighbor fractures along the main directions of flow in a fractured block. All the  
376 geometrical methods need the detailed geometry of the DFN, although OBS could be used  
377 without it (See Section 2). But for a fair comparison we assume for all methods that the  
378 skeleton of the fracture network is known.

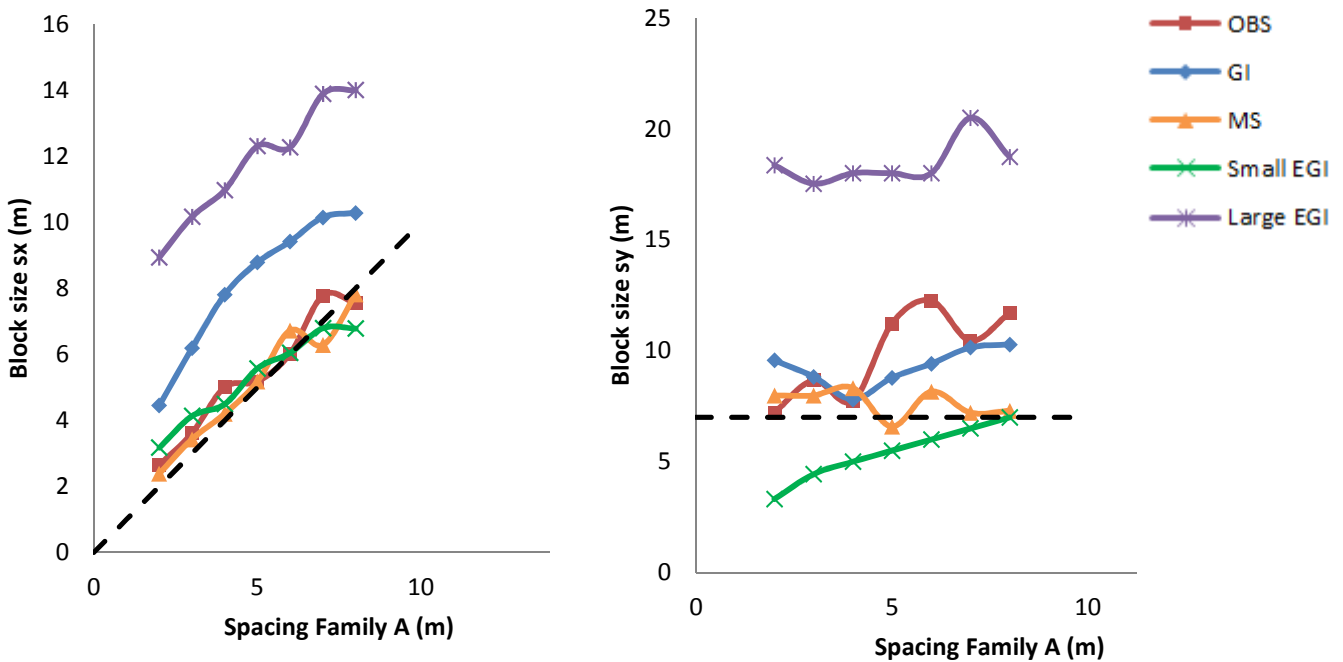
379 The comparison of OBS, GI, EGI, and MS is conducted for the two horizontal  
380 directions of a three-dimensional fractured block (100 m on a side) consisting of two families  
381 of near-vertical fracture planes. In the first test, a fracture family denoted *A*, is oriented with  
382 an azimuth of  $100^\circ$  counted positive anticlockwise from the main direction  $x$  of the fractured  
383 block. The second fracture family denoted *B* is oriented  $10^\circ$ . The spacing between fractures of  
384 family *B* is kept constant at 7 m, as the spacing of family *A* is varied between 2 and 8 m for  
385 different realizations of the DFN (two examples reported in Fig. 3).



**a** **b**  
386 Fig. 3. Examples of random discrete fracture networks (DFN) with two near-vertical fracture  
387 families at the scale of a reservoir grid cell. The azimuths of family *A* and *B* are  $100^\circ$  and  $10^\circ$ ,  
388 respectively. DFN a: family *A* (resp. *B*) with mean spacing of 2 m (resp. 7 m); DFN b:  
389 families *A* and *B* with mean spacing of 7 m.

390

391 If we denote as  $s_x$  and  $s_y$  the mean matrix block sizes along the  $x$  and  $y$  horizontal directions  
 392 of the fractured block, in view of the orientations of fracture families  $A$  and  $B$ ,  $s_x$  should be  
 393 close to the mean spacing of  $A$  (i.e., 2 – 8 m), and  $s_y$  close to the spacing of  $B$  (i.e., 7 m). Fig.  
 394 4 reports on sought values of  $s_x$  and  $s_y$  for different methods of calculation with specifically  
 395 the EGI technique rendering two sets of measures (see Appendix B) - small-EGI, large-EGI –  
 396 as the technique assumes the existence of two types of matrix block interacting with the  
 397 fracture network during flow.



**a** **b**  
 398 Fig. 4. Mean matrix block sizes  $s_x$  and  $s_y$  as functions of the spacing of fracture family  $A$   
 399 (fracture networks in Fig. 4) for different methods of calculation. OBS = oriented block size  
 400 method, GI = general imbibition method, EGI = enhanced general imbibition method (with  
 401 "small" and "large" sizes of matrix blocks), and MS = mean spacing method.

402  
 403 In general, the OBS calculations retrieve the expected values of  $s_x \approx 2-7$  m as a  
 404 function of the spacing of fracture family  $A$  (Fig. 4a). The size  $s_y$  which should be constant at

405 7 m, actually evolves with the spacing of family *A* and is overestimated of 10% to 50% (Fig.  
406 4b). This overestimation cannot be the consequence of an actual fracture network that would  
407 be far from a regular WR representation since the actual network is simple and made of two  
408 perpendicular fracture families with directions almost parallel to the  $x$  and  $y$  directions of the  
409 fractured block. Nevertheless, we noted that increasing the spacing of the fracture family *A*  
410 also diminished the connectivity of the DFN with a few subdomains almost free of any  
411 fracture and poorly connected to the facets of the fractured block. It is noteworthy that  
412 estimates of effective properties of the DFN, especially porosities (or their influence on  
413 macroscopic permeabilities in Eq. (15)), both at the facets and inside the block are key  
414 features to the OBS calculations (see Section 2). Since less connected networks return weaker  
415 porosity values, the equivalent WR network assigned with those porosities will contain less  
416 fractures and result in increased matrix block sizes extracted from the equivalence between  
417 the WR network and the DFN.

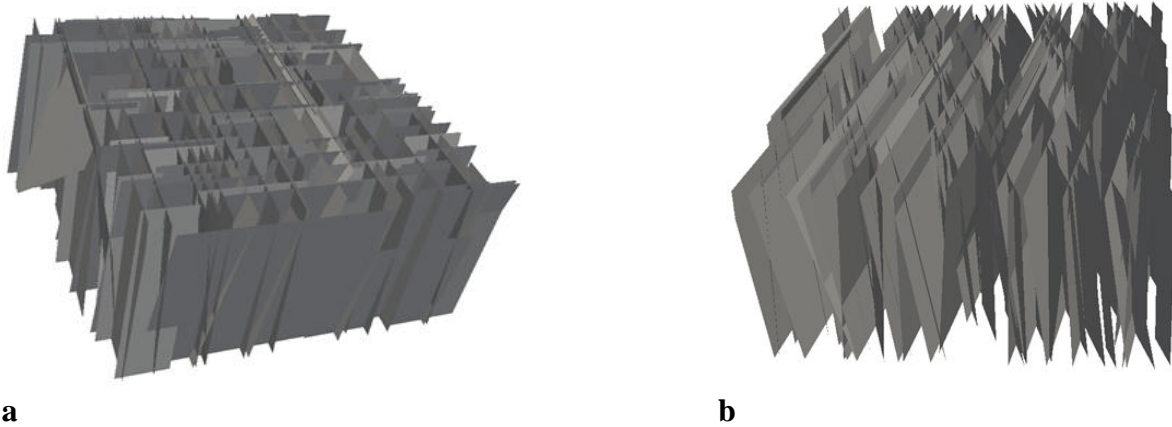
418         Compared with the expected values, matrix block sizes  $s_x$  and  $s_y$  extracted from the  
419 GI technique tend to be overestimated. This result is foreseeable because GI usually  
420 experiences some difficulties when dealing with DFN encompassing both small and large  
421 matrix blocks. These difficulties are the consequence of the oversimplified fitting with a  
422 second degree polynomial of the so-called invasion area curve calculated by the method as the  
423 surface area in the matrix domain located at a given distance from the closest fracture of the  
424 system (see Appendix *B*). Regarding EGI, the "small block" estimates  $s_x$  are in the correct  
425 range 2-8 m when the size  $s_y$  is always overestimated. For their part, the "large block"  
426 estimates in EGI are always more than twice the expected values. Finally, the MS method  
427 infers correct values of  $s_x$  and  $s_y$  whichever the investigated DFN and the spacing of fracture  
428 families *A* and *B*. Notably, the MS method is weakly influenced by the fracture network  
429 connectivity which might become a drawback when dealing with sparse and poorly connected

430 fracture networks. In that case MS will still measure the mean lag distance separating two  
431 neighbor fractures, as a poorly connected network tends to conceal a few cluster of large  
432 matrix blocks in the system. In that case mean matrix block sizes from MS would be  
433 underestimated.

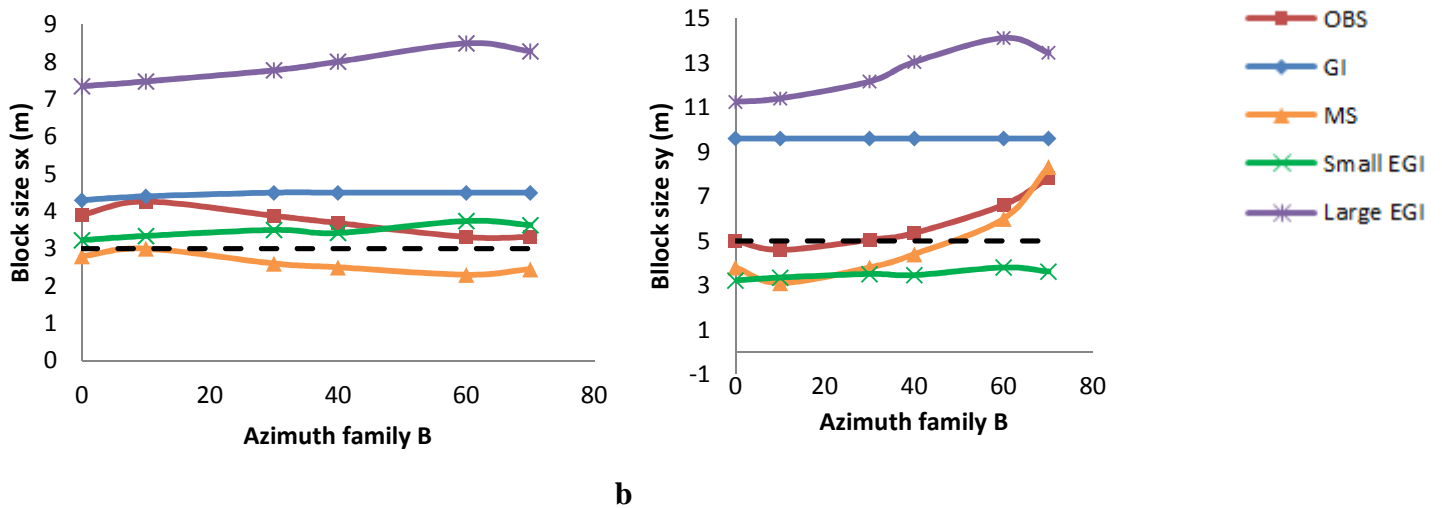
434 In the OBS technique, whose specificity is seeking the equivalence between the actual  
435 DFN and a regular WR network, this equivalence seems intuitively easier to achieve for  
436 DFNs with fracture families whose principal orientations are close to the main directions of  
437 the whole block. Therefore, it makes sense to address the capabilities of the method under less  
438 favorable conditions where actual fractures do not line up with the main block directions. We  
439 re-handled the comparison of matrix block sizes drawn from fracture networks still made of  
440 two almost vertical fracture families, but this time with a constant spacing of 3 m for family  
441 A, 5 m for family B, and varying the orientation of the families with respect to the main  
442 directions  $x$  and  $y$  of the block. The fracture family A is still oriented  $100^\circ$  (counted positive  
443 anticlockwise) with respect to the  $x$  direction and the orientation of family B is varied between  
444 0 and  $70^\circ$  with respect to  $x$  (Fig. 5). In view of the geometrical settings of the DFNs, the  
445 matrix block size  $s_x$  should be close to 3 m and  $s_y$  close to 5 m when the fracture family B is  
446 almost orthogonal to family A (azimuth of B =  $0-10^\circ$ ). Block sizes  $s_x$  should then slightly  
447 decrease as  $s_y$  should increase when the direction of fracture family B departs from  
448 orthogonality with A.

449 The GI method systematically overestimates both  $s_x$  and  $s_y$  in each configuration of  
450 the fracture network. The EGI technique still tends to overestimate  $s_x$  and  $s_y$  with its "large  
451 block" measure while correct or slightly underestimated values are found with the "small  
452 block" measure. In any case, both GI and EGI are weakly sensitive to the fracture family  
453 orientations with almost constant values  $s_x$  and  $s_y$  irrespective of the azimuth prescribed to

454 fracture family  $B$  in the DFN (Fig. 6). This result is consistent with the fact that both  
 455 techniques model the surface occupied by matrix domains in the fractured block as a function  
 456 of the distance to the nearest fracture (Appendix B). This measure reveals far less sensitive to  
 457 fracture orientations than to fracture spacing.



458 Fig. 5. Examples of random discrete fracture networks (DFN) with two near-vertical fracture families at the scale  
 459 of a reservoir grid cell. The mean spacing of fracture families  $A$  and  $B$  are prescribed at 3 m and 5 m,  
 460 respectively, while the azimuth of family  $A$  is kept at  $100^\circ$  and the azimuth of family  $B$  is varied between  $0^\circ$   
 461 ( $DFN$  a) and  $70^\circ$  ( $DFN$  b).  
 462



463 Fig. 6. Mean matrix block sizes  $s_x$  and  $s_y$  as functions of the azimuth of fracture family  $B$  (fracture networks  
 464 in Fig. 5) for different methods of calculation. OBS = oriented block size method, GI = general imbibition  
 465 method, EGI = enhanced general imbibition method (with "small" and "large" sizes of matrix blocks), and MS =  
 466 mean spacing method.

467           The MS and OBS techniques infer very similar matrix block size values, these being  
468 sometimes slightly underestimated by MS and slightly overestimated by OBS. For azimuths  
469 of the fracture family  $B$  between 0 and 45°, the estimated  $s_x$  with both MS and OBS are close  
470 to the expected value of 3 m and stay almost constant whichever the orientation of family  $B$ .  
471 Concerning  $s_y$ , the expected value of 5 m is retrieved by OBS and underestimated at 3-4 m  
472 by MS. For azimuths of the fracture family  $B$  between 45 and 70°, both methods return, as  
473 expected,  $s_x$  values that slightly decrease, as  $s_y$  values increase from approximately 5 m up  
474 to 8 m. OBS mainly captures the projection of the fracture planes onto the facets delimiting  
475 the fractured block (see Section 2 and Appendix A), which is obviously sensitive to fracture  
476 orientations. In the same vein, MS evaluates the mean distance between fractures along the  
477 main directions of the fractured block with the obvious consequence of increasing the  
478 apparent distance when fracture planes are not normal to the direction of measure.  
479 Nevertheless, both methods provide valuable results for dense fracture networks or fractured  
480 blocks wide enough to enclose a large number of fractures allowing for significant statistical  
481 measures of fracture spacing (MS) or block-side and inner-block hydraulic properties (OBS).

482           Notwithstanding other considerations such as computation times (see hereafter), OBS  
483 and MS techniques seem to outperform GI and EGI in extracting mean matrix block sizes  
484 from fractured system. We noted however that OBS is sensitive to the loss of connectivity in a  
485 fracture network with the consequence of increasing the inferred matrix block size. This  
486 artificial increase might result in biased evaluations of fluid flux exchanges between fracture  
487 and matrix media. Numerical exercises comparing discrete fracture network outputs and their  
488 dual porosity representation with OBS-sized matrix blocks are conducted to answer this  
489 question. The other geometrical techniques GI, EGI, and MS are also tested. We remind that  
490 these three numerical techniques are in essence only applicable when a prior knowledge of the  
491 fracture network geometry is available, while the OBS technique might be applied either on



492 known or unknown geometries (see Section 2). For a fair comparison of all techniques  
493 hereafter, we consider that the fracture network geometry is known.

494

#### 495 **4. Two-dimensional numerical test cases**

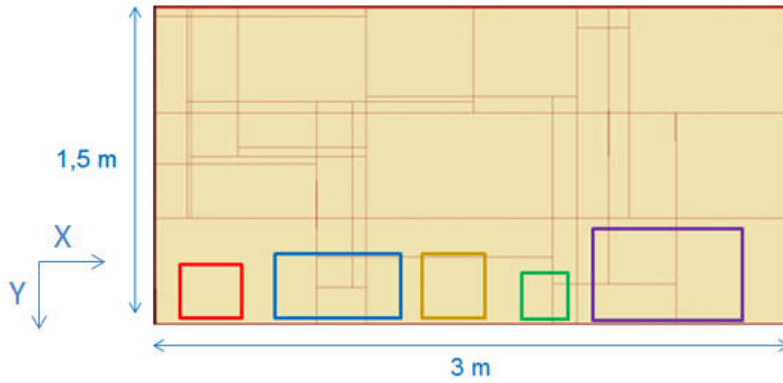
496 As already mentioned, dual continua representations of discrete fracture networks are  
497 conducive to drastic reductions in computation costs but require carefully designed settings to  
498 adequately represent both conductive and capacitive properties of a fractured porous medium  
499 subject to Darcian flow. We address here two phase flow in both DFN and dual porosity  
500 models. The setup of calculations is dimensioned to represent large laboratory analogs of  
501 flow in fractured media as conducted for instance in "Hele-Shaw" cells (e.g., Park and  
502 Homsy, 1984; Folch et al., 1999). We remind that we are interested in the assessment of mean  
503 matrix block size from different geometrical-structural techniques that always manipulate  
504 relative quantities as the spacing of fractures compared to the block size, or fracture traces  
505 intercepted by block facets. Therefore, our findings from numerical experiments at the scale  
506 of a lab device should not be hampered by loss of generality. In addition, we perform  
507 calculations, especially in the context of DFN discretization, over synthetic fracture networks  
508 with regular fracture orientations. This choice reduces discretization efforts but is mainly  
509 employed herein because it ensures accuracy of reference calculations in a DFN compared  
510 with that from a dual porosity model. Even though sophisticated meshing techniques and  
511 advanced numerical methods exist, it was found that thin fracture elements in unstructured  
512 meshing tend to smear the calculation of their state variables over the large matrix blocks.  
513 This feature is not suited to compare (local) DFN and (large scale) dual porosity calculations  
514 of diffusive flow.

515 Numerical simulations are performed over two-dimensional horizontal fractured  
516 systems (of unit thickness) that only neglect gravity-driven flow. Notably, the various

517 techniques employed in this study to calculate mean matrix block sizes are not sensitive to  
518 gravity-driven flow and only manipulate geometrical considerations on the fracture network  
519 or equivalences in permeability-porosity between an actual fractured block and a sugar-cube  
520 model. Two-phase flow in a DFN is performed over a fractured system of 3 m length and 1.5  
521 m width finely discretized by 11590 square elements for an accurate representation of both  
522 the fracture network and matrix. The system is also roughly discretized by only 920 square  
523 elements of a dual-porosity, single-permeability model with matrix block sizes extracted from  
524 the DFN via the EI, EGI, MS and OBS techniques (see Section 3). Two-phase flow is  
525 numerically solved by means of a finite volume technique and uses an implicit-in-time  
526 scheme for time integration of the pressure equation while an explicit-in-time scheme is used  
527 for time integration of either the water or oil mass balance. To avoid unfair comparisons  
528 between GI, EGI, MS, and OBS, a simple fracture network is delineated with fractures only  
529 parallel to the main flow directions  $x$  and  $y$  of the system. Dead ends of the fracture network  
530 are also removed since in essence they are always accounted for in the fracture-matrix  
531 relationship by GI and EGI methods when MS and OBS might not see these dead-ends  
532 because they are not counted in MS or do not participate to side-block properties in OBS.

533         The first fractured system investigated (Fig. 7) is initially saturated with oil and  
534 percolated by water injected from the western boundary taken as a Neumann condition  
535 prescribing a constant-in-time water flux. The eastern boundary of the system is of Dirichlet  
536 type while North and South boundaries are of no-flow type. Table 1 indicates the local  
537 hydraulic properties of each medium (fractures, matrix) in the DFN, Table 2 reports on inner-  
538 block and block-side properties used by the OBS method to calculate matrix block sizes, and  
539 Table 3 gathers the various matrix block sizes  $s_x$  and  $s_y$  obtained from the GI, EGI, MS and  
540 OBS methods.

541



542

543 Fig. 7. Two-dimensional fracture network serving as a system finely discretized or handled as a dual-porosity  
 544 model for the purpose of flow dynamics comparison. The size of matrix blocks in a dual porosity approach are  
 545 reported as colored frames, from left to right: Red = oriented block size method, Blue = general imbibition  
 546 method, Orange = mean spacing imbibition method, Green and Purple = small and large sizes from enhanced  
 547 general imbibition method.

548

	Matrix medium	Fractures
Porosity $\phi$ [-]	0.1	1
Permeability $k$ [ $10^{-15} \text{ m}^2$ )]	1 and 10	10000
Relative permeability $k_r$ [-]	<p>Brooks Corey (<math>\lambda=2</math>)</p>	<p>"Cross" <math>k_r</math></p>
Capillary pressure $P_c$ [bar = $10^4 \text{ kgms}^{-2}$ ]	<p>Brooks Corey (<math>\lambda=2</math>)</p>	Null capillary pressure

549 Table 1. Set up of main flow parameters for calculations of two-phase flow in fractured systems depicted in Fig.  
 550 7 and 10. The relative permeability and capillary pressure as functions of water saturation in the matrix obey the  
 551 Brooks and Corey model (1964) with  $\lambda$  ( $=2$ ) the so-called pore-size distribution index.

552

	x direction	y direction
$k_f$ [ $10^{-15}$ m <sup>2</sup> ]	46.42	120
$k^{FN-S}$ [ $10^{-15}$ m <sup>2</sup> ]	40	120
$\phi^{FN-S}$ [-]	0.004	0.012
$\phi_f$ [-]	0.012	

553 Table 2. Main macroscopic parameters of the fractured block in Fig. 7 to infer via the oriented block size  
 554 technique the mean matrix block size of a dual porosity model.  $k_f$ ,  $\phi_f$  respectively are the permeability and  
 555 porosity of the whole block,  $k^{FN-S}$ ,  $\phi^{FN-S}$  respectively are the permeability and porosity of the fracture  
 556 network at the sides (normal to  $x$  and  $y$  directions) of the block.

557

Block sizes	OBS	GI	MS	EGI- large	EGI- small
$s_x$ [m]	0.360	0.6	0.35	0.696	0.257
$s_y$ [m]	0.306	0.3	0.345	0.494	0.257

558 Table 3. Mean matrix block sizes of a dual porosity model as a surrogate to the discrete fracture network in Fig.  
 559 7.

560

561 Two different types of flow are simulated, the first one with low water injection rate of  
 562 0.1 m/day in the fractures and low matrix permeability of  $10^{-15}$  m<sup>2</sup>, the second one with higher  
 563 injection rate of 1 m/day and higher matrix permeability of  $10^{-14}$  m<sup>2</sup>. On the one hand, the  
 564 first scenario with small water fluxes in the fractures and weakly permeable matrix enhances  
 565 capillary effects as the origin of pressure gradients between fracture and matrix and  
 566 subsequent exchange rates between both media Due to capillary effects in the matrix and  
 567 absence of these in the fractures, the oil pressure in the matrix is higher than that in the  
 568 fractures and oil is ejected from the matrix (or water invades the matrix). On the other hand,  
 569 the second scenario with high injection velocities favors "piston" flow in the fractures and  
 570 enhances fracture-matrix exchanges as the consequence of the excess of water pressure in  
 571 fractures compared with oil pressure in the matrix. Water invades the matrix and the process

572 is enhanced by the contrast of mobility (the ratio  $kr/\mu$ ) between oil and water phases which  
 573 triggers rapid water invasion along the fractures and early leaching of matrix blocks.

574 To reinforce these assertions about flow scenarios with contrast between capillary and  
 575 viscous forces to extract oil from matrix blocks, we also calculated a dimensionless capillary  
 576 number based on the evaluation of water fluxes invading matrix blocks versus expulsion of oil  
 577 from the matrix to fractures by capillary pressure contrasts. With steady-state flow sweeping  
 578 oil from the system by forced water injection at one side of the fractured block, the mean  
 579 water pressure gradient in the system is evaluated as

$$580 \quad |\nabla P_w| \approx \frac{V_{inj} \mu_w}{k_i^f} \quad (15)$$

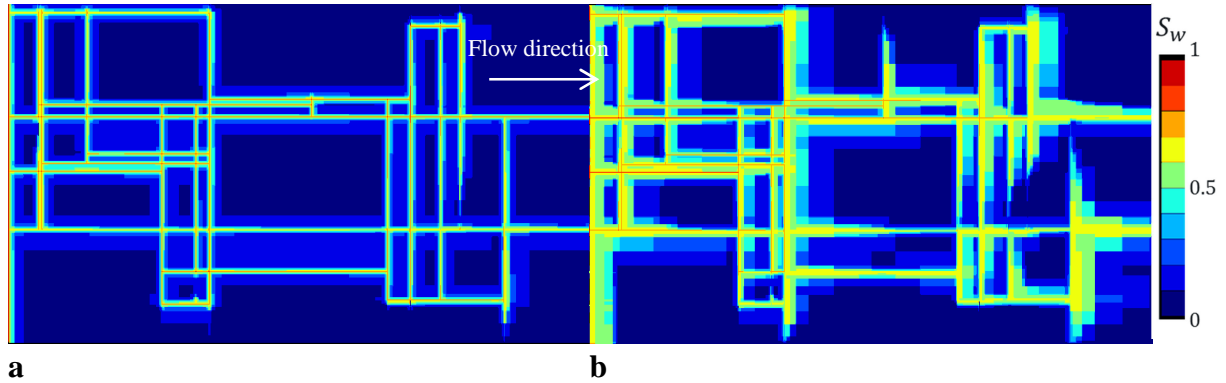
581  $P_w$  [ $ML^{-1}T^{-1}$ ] is the water pressure in both the fractures and the matrix,  $V_{inj}$  [ $LT^{-1}$ ] is the  
 582 injection velocity of water at the upstream side of the fractured block,  $\mu_w$  [ $ML^{-1}T^{-1}$ ] is the  
 583 dynamic viscosity of water, and  $k_i^f$  [ $L^2$ ] is the equivalent fracture permeability of the whole  
 584 block along the direction  $i$  of water injection. Regarding the capillary pressure gradient, we  
 585 assume a null capillary pressure in the fractures (open medium of unit porosity) and we take  
 586 in the matrix the maximal capillary pressure  $P_c^{\max}$  given by relationships capillary pressure –  
 587 saturation (see, e.g., Table 1). The capillary pressure gradient between matrix and fractures is  
 588 then approximated as

$$589 \quad |\nabla P_c| \approx \frac{P_c^{\max}}{s_{\min}/2} \quad (16)$$

590 with  $s_{\min}$  [L] the smallest dimension (in either directions  $x$ , or  $y$  or  $z$ ) of the mean matrix  
 591 block size. A dimensionless capillary number balancing capillary gradient with water pressure  
 592 gradient can be expressed as

$$593 \quad n_c = \frac{|\nabla P_c|}{|\nabla P_w|} \approx \frac{2P_c^{\max} k_i^f}{s_{\min} \mu_w V_{inj}} \quad (17)$$

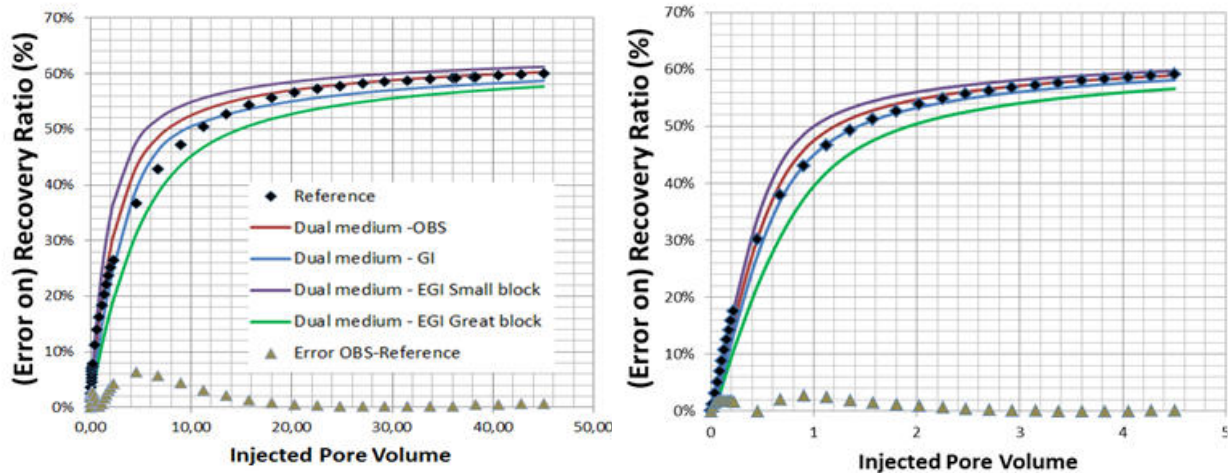
594 This capillary number is larger than one for flow conditions dominated by capillary forces as  
595 it becomes close to one or less than one when viscous forces condition flow in the fractured  
596 block.



597 Fig. 8. Maps of water saturation in a water-flooding two-phase flow scenario. Calculations are performed over a  
598 fine grid discretizing both the fracture network and matrix (system in Fig. 7). The system is initially saturated in  
599 oil and water is injected in the fractures at a constant flow rate at the western boundary of the system. Oil  
600 recovery is monitored at the eastern boundary (see Fig. 9). The fluid exchange between fractures and matrix is  
601 dominated by capillary forces in map *a* as both capillary and viscous forces are active in map *b*.

602  
603 In the DFN approach where matrix-fracture exchanges are dominated by capillary  
604 effects ( $n_c = 4.1$  with the settings of the simulations), water does not deeply invade the  
605 matrix (Fig 8.a,) while for the same injected water pore volume, high injection velocity and  
606 piston flow ( $n_c = 0.41$ ) maintains higher water pressure gradients that help to a deeper water  
607 invasion of the matrix (Fig. 8.b). Calculations in the DFN serve as reference to the  
608 comparison of flow scenarios between dual porosity models assigned with matrix block size  
609 from the GI, EGI, MS and OBS methods (sizes of blocks are pictured in Fig. 7). The  
610 comparison is here performed by way of a single indicator defined as the evolution in time  
611 (precisely, the evolution with the water pore volume injected in the system) of the oil  
612 recovery ratio at the outlet of the fractured system. This oil recovery corresponds to the ratio  
613 of the cumulative volume of oil exiting the system to the total initial volume of oil in the  
614 system. This indicator is obviously macroscopic, with the meaning that it monitors the

615 behavior of the system at the large scale (at least the homogenization scale of the fracture  
 616 network). It would not make sense to compare a local feature of the fracture network (e.g., the  
 617 pressure transients in a single fracture) with averaged behaviors obtained for the large blocks  
 618 (cells) of a dual porosity approach.  
 619



**a**

**b**

620 Fig. 9. Oil recovery ratio versus water injected pore volumes at the eastern boundary of a fractured network (in  
 621 Fig. 7). The so-called reference is calculated by means of a finely discretized network as the other curves are  
 622 drawn from a dual porosity model with various mean matrix block sizes. Results from the mean spacing  
 623 technique for matrix block size evaluation are not reported because they are merged with those from the oriented  
 624 block size technique. Capillary forces dominate the exchange rate between fractures and matrix in plot *a*, as both  
 625 capillary and viscous forces are active in plot *b*.  
 626

627 Fig. 9 presents two plots of the oil recovery ratio as a function of the injected pore  
 628 volume and stemming from flow scenarios with low and high injection velocities. The same  
 629 oil recovery ratio of approximately 60% is reached for both flow scenarios, but with only 5  
 630 pore volumes in the case of high injection velocity compared with the 50 pore volumes  
 631 required by the case of low injection velocity. No dual porosity model with their different  
 632 matrix block size renders results that completely depart from the reference calculations in the  
 633 DFN. Since matrix block sizes calculated with OBS and MS techniques are quite similar (see

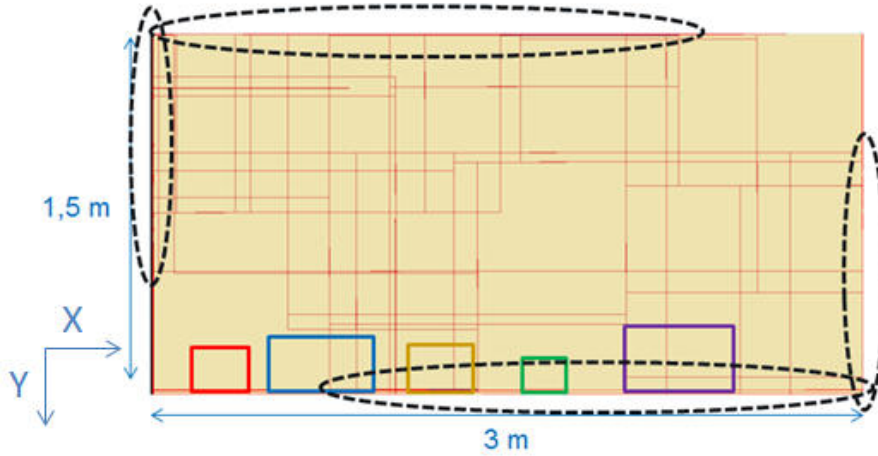
634 Fig. 7 and Table 3), the results from dual porosity model simulations do not differ  
635 significantly and only outputs from the OBS technique are reported in Fig. 9.

636 The OBS technique tends to slightly underestimate the matrix block size which  
637 triggers a quicker oil extraction from the matrix and produces recovery curves slightly shifted  
638 toward short injection times. The simulations handling the GI matrix blocks are also in very  
639 good agreement with references, especially in the case of fracture-matrix exchanges enhanced  
640 by high water injection rate. The matrix block sizes of EGI are still underestimated by the  
641 "small block" measure and overestimated by the "large block" measure giving rise to  
642 respectively faster and slower evolutions of the oil recovery ratio with respect to time. As  
643 such, the EGI technique is not the most accurate to calculate matrix block sizes and should be  
644 employed as a convenient way to provide minimal and maximal bounds to these sizes.  
645 Notably, the fractured system discussed above does not significantly distinguish between GI  
646 and OBS in terms of accuracy whichever the mechanism prevailing in fluid flux exchanges  
647 between fractures and matrix. Nevertheless, we are reminded that the reference fracture  
648 network was built to mitigate GI downsides. Fracture dead-ends were removed from the  
649 network and the two fractures families were set parallel to the  $x$  and  $y$  directions of the  
650 fractured block, thus allowing the GI method to infer a precise "invasion curve" ( $A(X)$  in  
651 Appendix B). This is why GI shows good performances in the present test cases as it  
652 exhibited more discrepancies in the geometrical test cases discussed in Section 3.

653 At this stage, it must be raised that the OBS technique partly relies upon evaluations of  
654 block-side properties such as fracture porosity and permeability, the latter being eventually  
655 not representative of inner-block quantities when the portion of fractures intercepting the  
656 block sides are not representative of the network geometry inside the block. To address the  
657 eventual influence of this downside, we recalculated the two flow scenarios discussed above  
658 for another fractured system (Fig. 10) which comprises a few long fractures located very close



659 to the sides of the system. These fractures delimit a few very elongated matrix blocks close to  
 660 the boundaries of the system (those encircled in Fig 10) as the majority of matrix blocks  
 661 inside the system are rectangular with a ratio length to width barely exceeding a factor 3. As  
 662 expected, the inner-block and block-side properties used by the OBS method (Table 4) differ  
 663 from that of the fractured "regular" system previously discussed.



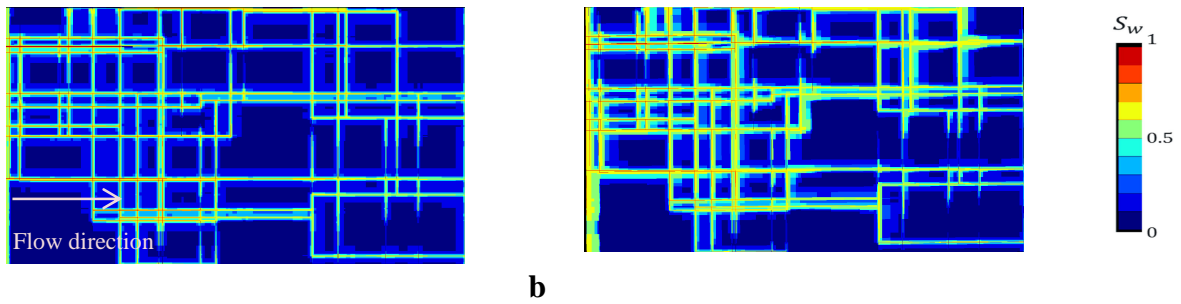
664 Fig. 10. Two-dimensional fracture network serving as a system finely discretized or handled as a dual-porosity  
 665 model. Fractures close to the boundaries delimit very narrow matrix blocks (encircled) that depart from the shape  
 666 of blocks within the fracture network. The identified sizes of matrix blocks in a dual porosity approach are  
 667 reported as colored frames, from left to right: Red = oriented block size method, Blue = general imbibition  
 668 method, Orange = mean spacing imbibition method, Green and Purple = small and large sizes from enhanced  
 669 general imbibition method.  
 670

671

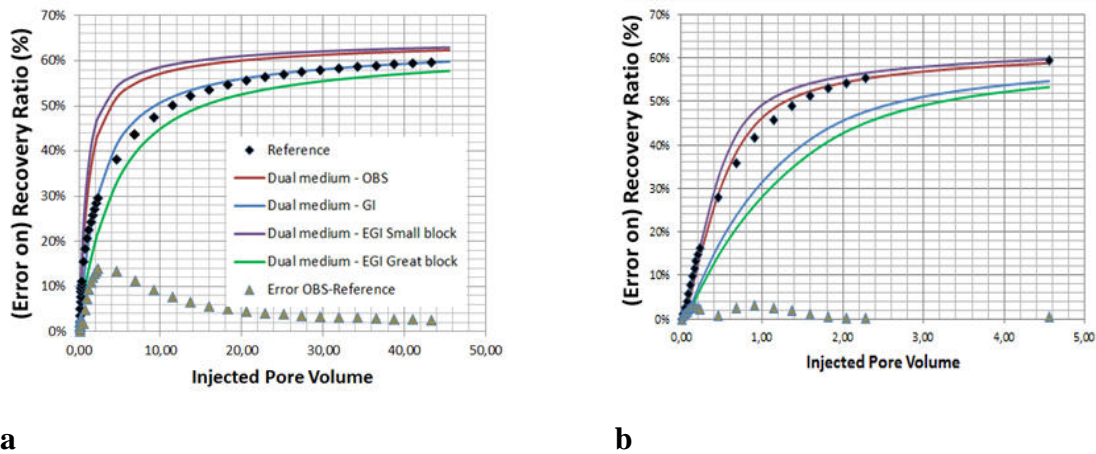
	x direction	y direction
$k_f [10^{-15} \text{ m}^2]$	107.72	240
$k^{FN-S} [10^{-15} \text{ m}^2]$	106.66	240
$\phi^{FN-S} [-]$	0.0106	0.024
$\phi_f [-]$	0.024	

672 Table 4. Main macroscopic parameters of the fractured block in Fig. 10 to infer via the oriented block size  
 673 technique the mean matrix block size of a dual porosity model.  $k_f$ ,  $\phi_f$  respectively are the permeability and  
 674 porosity of the whole block,  $k^{FN-S}$ ,  $\phi^{FN-S}$  respectively are the permeability and porosity of the fracture  
 675 network at the sides (normal to x and y directions) of the block.

676 Comparing reference calculations performed over the DFN (maps of water saturation  
 677 in the system reported in Fig. 11, capillary number  $n_c$  of 19 for Fig. 11a and of 1.9 for Fig  
 678 11b) and calculations in the dual porosity models reveals that the oil recovery ratio is still of  
 679 approximately 60% after 4-5 injected pore volumes for high injection velocity and 40 pore  
 680 volumes under low injection velocity conditions (Fig. 12).



681 Fig. 11. Maps of water saturation in a water-flooding two-phase flow scenario. Calculations are performed over a  
 682 fine grid discretizing both the fracture network and matrix (system in Fig. 10). The system is initially saturated in  
 683 oil and water is injected in the fractures at a constant flow rate at the western boundary of the system. Oil  
 684 recovery is monitored at the eastern boundary (see Fig. 12). The fluid exchange between fractures and matrix is  
 685 dominated by capillary forces in map a as both capillary and viscous forces are active in map b.  
 686



687 Fig. 12. Oil recovery ratio versus water injected pore volumes at the eastern boundary of a fractured network (in  
 688 Fig. 10). The reference curve is calculated by means of a finely discretized network as the other curves are drawn  
 689 from a dual porosity model with various mean matrix block sizes. Results from the mean spacing technique are  
 690 not reported because they are merged with those from the oriented block size technique. Capillary forces  
 691 dominate the exchange rate between fractures and matrix in plot a, as both capillary and viscous forces are active  
 692 in plot b.

693 This result confirms that the macroscopic behaviors of both the DFN and its  
694 representation as a dual porosity system are changed much by the few fractures that do not  
695 obey the general geometric and structural settings of the whole fractured block. This feature is  
696 also evidenced by the comparison between the maps of water saturation in Fig. 8 and Fig. 11  
697 that only differ by the locations of fractures underlined by high water saturations. However,  
698 discrepancies between the reference (taken as the DFN) and the dual porosity approximations  
699 increase. As for the preceding example, OBS and MS techniques provide very similar matrix  
700 block sizes (these sizes are pictured in Fig. 10 and reported in Table 5) and similar dual-  
701 porosity behaviors making that MS results are not discussed in the following.

702

Block sizes	OBS	GI	MS	EGI- large	EGI- small
$s_x$ [m]	0.185	0.44	0.24	0.47	0.147
$s_y$ [m]	0.149	0.21	0.19	0.325	0.138

703

704 Table 5. Mean matrix block sizes of a dual porosity model as a surrogate to the discrete  
705 fracture network in Fig. 7.

706

707 In the case of matrix-fracture exchanges dominated by capillary forces (Figs 11a, 12a)  
708 the OBS technique overestimates the leaching of matrix block ( and oil production at the  
709 outlet of the system) because the smallest matrix block size (here along the y direction) is  
710 underestimated. Whichever the algebraic form chosen in OBS to infer the matrix block size  
711 (See Section 2), the method is in essence sensitive to fracture densities close to the boundaries  
712 of the whole fractured block, either in regard of porosities at the sides of the block or of  
713 permeability values in a "permeameter" type system. If the actual matrix block sizes close to  
714 the boundaries of the block are smaller than inside the block, as is the case with the present  
715 example, the smallest matrix block size (here along y, see Table 5) is underestimated which

716 favors rapid imbibition under capillary forces (see above the capillary number  $n_c$ ). Notably,  
717 the GI technique is not sensitive to the few small matrix blocks of the DFN because it treats  
718 the shell and inner parts of the block exactly the same way. For its part, the "small" EGI  
719 technique underestimates the mean matrix block size as the "Large" EGI overestimates it  
720 ("small" EGI overestimates matrix imbibition and "Large" EGI underestimates imbibition, see  
721 oil recovery in Fig. 12a compared with reference).

722         When matrix-fracture exchanges occur as a conjunction of viscous and capillary forces  
723 (see the capillary number in (17) and subsequently evaluated for DFN simulations), the OBS  
724 technique renders results the closest to reference. The key is that rapid water invasion of the  
725 fractured block through permeable fractures (see Fig. 11b) and subsequent viscous effects  
726 between matrix and fractures are dominated by percolation through the large fractures and  
727 their (large) neighbor matrix blocks. As the OBS technique identifies the correct largest  
728 matrix block size (here along the  $x$  direction, see Table 5), flow simulations with a dual  
729 porosity model are convincing. This time, the GI technique underestimates oil recovery, as  
730 "Large" EGI does too, because the overestimated matrix block size (especially along the  $x$   
731 direction, see Table 5) is favorable to capillary imbibition but hampers water invasion along  
732 fractures and matrix block leaching at early injection times.

733         Finally, regarding performances in terms of computation costs, the different geometric  
734 methods were applied to a large DFN represented as a synthetic dual porosity reservoir of  
735 1.05 million grid cells. For OBS and MS methods, matrix block size calculations were  
736 performed for each elementary cell and duplicated over all cells of the reservoir with total  
737 CPU times coming up as: 230 s for OBS and 1120 s for MS. Notably, the time counted for GI  
738 and EGI is that of calculations over a limited number of cells "strategically" sampled in the  
739 whole grid of the dual porosity reservoir, yielding a fair representation of the system after  
740 1800 s of calculation. With approximately 4 s of calculation per cell and  $10^6$  cells, identifying

741 a matrix block size for each cell with GI and EGI methods would render impracticable  
742 evaluations exceeding 45 days. When applied to known DFNs, both OBS and MS require a  
743 pre-evaluation of the diagonal permeability tensor of the fractured block; by construction for  
744 OBS (see Section 2) and to identify main flow directions in MS for which random lines  
745 counting the spacing of fractures (see Appendix B) are parallel to these directions.  
746 Differences of computations times between methods are in the straightforward (and fast)  
747 application of an analytical solution for OBS opposed to the need for many random draws in  
748 MS.

749

## 750 **5. Conclusions**

751 The Oriented Block Size (OBS) technique has been developed as a new way to infer  
752 the mean matrix block sizes in porous fractured media with application to dual porosity  
753 models of flow at the large scale. Matrix block sizes are calculated by seeking the equivalence  
754 in terms of fracture permeability and fracture porosity between a fractured block and a  
755 Warren and Root discrete fracture network made of three fracture families with regular  
756 spacing and fracture planes normal to the main flow directions.

757 Two expressions of the OBS are available according to which type of fractured block  
758 the method is applied. The first expression is well suited to infer matrix block sizes over  
759 synthetic discrete fracture networks or well-known actual networks since it requires  
760 identifying fracture porosity of the network, fracture porosity at the sides of the fractured  
761 block, and the diagonal permeability tensor of the whole block (which can be calculated  
762 analytically or numerically). This first expression is based on a rigorous algebraic  
763 development which reveals precise and renders matrix block sizes close to expectations drawn  
764 from various synthetic discrete fracture networks. The second expression is derived from the  
765 first one via assumptions on the fracture porosities of the block. It has the advantage of being

766 applicable to hardly accessible fracture network as encountered in the field. This second  
767 expression is compatible with an inference from field measurements such as hydraulic tests  
768 and observations in wells but should only render orders of magnitude instead of pinpoint  
769 values. Further works should address how matrix block sizes are influenced by uncertainty on  
770 available field data.

771         The OBS technique revealed much faster in terms of computation times compared  
772 with other available geometrical techniques developed to infer matrix block sizes. This feature  
773 is a promising avenue for tentative applications of the method in up-scaling the representation  
774 of huge fractured reservoirs as done for instance in the oil industry when optimization of oil  
775 recovery from various exploitation scenarios is planned. In this context, OBS and its precise  
776 evaluation of matrix block sizes is useful to the parameterization of dual porosity models for  
777 two phase flow either dominated by capillary forces or viscous forces. However, as the other  
778 methods, the OBS technique may fail in retrieving matrix block sizes within poorly connected  
779 fracture networks. It is worth to note however that poorly connected networks are not valuable  
780 candidates to homogenization into a dual porosity model.

781         Finally, it must also be raised that OBS is associated with the identification of large  
782 scale permeability tensors that are mostly sensitive to the backbone of a fractured network and  
783 do not see fracture dead-ends. In the case of applications relying upon data from hydraulic  
784 well tests, the type of occurring flow should be carefully considered. Two phase flow, mostly  
785 witnessed by the propagation of an oil/water saturation front, will mainly record the effects of  
786 the backbone, as single phase flow, mainly monitored by the transient evolution of water  
787 pressure heads, would also be sensitive to dead-ends. It deserves some additional synthetic  
788 test cases or confrontation to actual field data to see whether or not the OBS technique reveals  
789 suited in these instances.

790

791 **Acknowledgments**

792 The authors are grateful to IFPEN for funding the Ph-D fellowship of C. Jerbi. They are also  
793 indebted to P. Delaplace at IFPEN for its fruitful advices provided all along this study.

794

795 **Appendix A. Matrix block sizes extracted from the equivalence between an actual**  
796 **fractured block and a Warren and Root (WR) block.**

797 We remind that an actual and well connected fractured block oriented with its main  
798 directions along the main directions of flow indexed by  $i=1,2,3$ , can be characterized by mean  
799 permeabilities  $k_i^{FN-S}$  along the sides of the block as

$$800 \quad k_i^{FN-S} = \frac{1}{2(\Delta_{i+1}\Delta_{i+2})} \left( \sum_{n=1}^{Nf_{i-}} k_n l_n e_n + \sum_{n=1}^{Nf_{i+}} k_n l_n e_n \right) \quad (A1)$$

801 The block size in direction  $i$  is denoted  $\Delta_i$  and the sides delimiting the block are also indexed  
802 by  $i$  but for limits normal to the main direction  $i$ . In addition, block sides are labelled  $i-$  or  
803  $i+$  according to their respective location upstream or downstream along direction  $i$ . In (A1),  
804  $i$  is a cycling index such that, e.g.,  $i+1 = 3$  when  $i = 2$  and  $i+1$  returns to 1 when  $i=3$ . The  
805 sides  $i-$  and  $i+$  of the block are intercepted by a number of fractures  $Nf_{i-}$  and  $Nf_{i+}$ , and  $k$   
806 is the local permeability of a fracture intercepting the side of the block over an apparent  
807 length  $l$  and with apparent fracture aperture  $e$ .

808 We also remind that a Warren and Root (WR) block concealing a regular fracture  
809 network of three fracture families can be characterized by two expressions associating: 1- the  
810 diagonal tensor of permeability of the whole block  $k_i^{WR}$  ( $i = 1, 2, 3$ ), 2- the mean porosity of the  
811 block  $\phi^{WR}$ , and 3- the porosity of the block sides  $\phi_i^{WR-S}$  ( $i = 1, 2, 3$ ), with the spacing  
812  $s_i$  ( $i = 1, 2, 3$ ), the aperture  $e_i$  ( $i = 1, 2, 3$ ), and the local permeability  $k_i$  ( $i = 1, 2, 3$ ) of the three  
813 fracture families composing the WR block (for details, see Section 2). These expressions are

$$814 \quad k_i = \frac{1}{2} \left( 1 + \frac{s_i}{e_i} \right) \sum_{j=1}^3 (-1)^{\delta_{i,j}} k_j^{WR} \quad (A2)$$

$$815 \quad k_i = \frac{1}{2(\phi^{WR} - \phi_i^{WR-S})} \sum_{j=1}^3 (-1)^{\delta_{i,j}} k_j^{WR} \quad (A3)$$



816 where  $\delta_{i,j}$  is the Kronecker symbol,  $\delta_{i,j} = 1, i = j; \delta_{i,j} = 0, i \neq j$ .

817 Following the idea that one can establish the equivalence between a WR network and  
818 an actual fractured block regarding their hydraulic properties, it is assumed that  $\phi^{WR}$ ,  $\phi_i^{WR-S}$ ,  
819 and  $k_i^{WR}$  are similar to the equivalent properties in the actual fractured block, respectively  
820 denoted as  $\phi^{FN}$ ,  $\phi_i^{FN-S}$ , and  $k_i^{FN-S}$  (see A1, for the latter). In the same vein, if a WR network  
821 serves as reference for fixing model parameters of homogenized approaches to fractured  
822 media, the characteristics of a WR network can be substituted by parameters of the  
823 homogenized model. For example, the characteristics  $s_i$ ,  $e_i$ , and  $k_j^{WR}$  in (A2) are respectively  
824 substituted by a mean matrix block size (also denoted  $s_i$  as defined in (3)), a mean fracture  
825 aperture  $e_f$ , and the entries of a diagonal tensor  $\mathbf{k}_j^f$  of the homogenized model. With these  
826 transformations, equating (A2) and (A3) results in

$$\begin{aligned}
 & \left(1 + \frac{s_i}{e_f}\right) \sum_{j=1}^3 (-1)^{\delta_{i,j}} k_j^f = \frac{1}{(\phi^{FN} - \phi_i^{FN-S})} \sum_{j=1}^3 (-1)^{\delta_{i,j}} k_j^{FN-S} \quad ; \quad i.e., \\
 827 \quad & s_i = e_f \left( \frac{\sum_{j=1}^3 (-1)^{\delta_{i,j}} k_j^{FN-S}}{(\phi^{FN} - \phi_i^{FN-S}) \sum_{j=1}^3 (-1)^{\delta_{i,j}} k_j^f} - 1 \right) \quad (A4)
 \end{aligned}$$

828 For the sake of simplification (see hereafter), the term  $-1$  in the expression of  $s_i$  can be  
829 dropped by considering that the term in  $(\phi^{FN})^{-1}$  is much larger than one for usual fracture  
830 porosity of a rock block barely exceeding a few percent. Stated differently, one might also  
831 consider in (A4) that the matrix block size  $s_i$  is much larger than the fracture aperture  $e_f$  and  
832 results in

$$833 \quad s_i \approx e_f \frac{\sum_{j=1}^3 (-1)^{\delta_{i,j}} k_j^{FN-S}}{(\phi^{FN} - \phi_i^{FN-S}) \sum_{j=1}^3 (-1)^{\delta_{i,j}} k_j^f} \quad (A5)$$

834 The mean matrix block size  $s_i$  in (A5) depends on both the mean fracture aperture  $e_f$   
835 and the fracture permeability of a homogenized model  $k_j^f$ . It is noteworthy that  $e_f$  is usually  
836 not a parameter of a homogenized approach, and it makes sense to render (A5) (partly)  
837 independent of any conjecture on the value of  $e_f$ . To this end, it is reasonably assumed that a  
838 WR network has its matrix block sizes separating neighbor fractures independent of the  
839 apertures  $e_i$  of the fractures. Stated differently, it is assumed that a WR network with a  
840 uniform aperture  $e_f$  for its three fracture families can be found as equivalent to a WR with its  
841 three fracture families with apertures  $e_i$ . With a uniform aperture  $e_f$ , a WR network would  
842 render a value  $\phi^{WR} - \phi_i^{WR-S} = e_f Nf_i / \Delta_i$  with  $Nf_i$  the number of fractures in the family  $i$ , and  
843  $\Delta_i$  the size of the whole fractured block along direction  $i$ . If the values  $\phi^{FN} - \phi_i^{FN-S}$  were not  
844 replacing their equivalent  $\phi^{WR} - \phi_i^{WR-S}$  in Eq (A5), the latter would no longer depend on  $e_f$ .  
845 Hence, our proposal is to calculate porosities of the actual fracture network by assigning the  
846 whole skeleton of the network with a constant single-fracture aperture  $e_f$ . The fracture  
847 network porosities for a constant aperture  $e_f$  would write as

$$848 \left( \phi^{FN} - \phi_i^{FN-S} \right) \Big|_{e=e_f} = e_f \left( \phi^{FN*} - \phi_i^{FN-S*} \right) \quad (A6)$$

849 The terms  $\phi^{FN*}$ ,  $\phi_i^{FN-S*}$  [ $L^{-1}$ ] denote porosities of the actual fracture skeleton per unit fracture  
850 aperture (that can be calculated by assigning a uniform fracture aperture of 1 to the whole  
851 fracture network). Substituting (A6) in (A5) simplifies the formulation of the matrix block  
852 size into

$$853 s_i \approx \frac{\sum_{j=1}^3 (-1)^{\delta_{i,j}} k_j^{FN-S}}{\left( \phi^{FN*} - \phi_i^{FN-S*} \right) \sum_{j=1}^3 (-1)^{\delta_{i,j}} k_j^f} \quad (A7)$$

854 The main characteristic of (A7) is that the mean matrix block size depends: 1- on a  
855 mean permeability tensor  $k_j^f$  of fractures at the scale of a (mesh of a) homogenized model of  
856 the system (e.g., a conjecture of the fracture permeability in a dual porosity model), 2- on the  
857 facet permeability values of the actual fracture network  $k_j^{FN-S}$ , and 3- on structural properties  
858 of the actual network resulting in fracture porosity values of the whole fractured block and its  
859 sides  $\phi^{FN*}$  and  $\phi_i^{FN-S*}$ , respectively. These features make that the form in (A7) is hardly  
860 applicable to poorly-known natural systems and should be mainly used in problems dealing  
861 with homogenization of systems with well-known geometry and discretization of synthetic  
862 fracture networks and matrix blocks.

863 Nevertheless, another form of the mean matrix block size can be proposed. By  
864 manipulating (A1), the permeability of the actual fracture network at the facets of the whole  
865 fractured block can be rewritten as

$$k_i^{FN-S} = \frac{\left( \sum_{n=1}^{Nf_{i-}} l_n e_n + \sum_{n=1}^{Nf_{i+}} l_n e_n \right)}{2(\Delta_{i+1} \Delta_{i+2})} \times \frac{\left( \sum_{n=1}^{Nf_{i-}} k_n l_n e_n + \sum_{n=1}^{Nf_{i+}} k_n l_n e_n \right)}{\left( \sum_{n=1}^{Nf_{i-}} l_n e_n + \sum_{n=1}^{Nf_{i+}} l_n e_n \right)} ; \text{ i.e.,}$$

866

$$k_i^{FN-S} = \phi_i^{FN-S} \bar{k}_i \quad \text{with} \quad \bar{k}_i = \frac{\left( \sum_{n=1}^{Nf_{i-}} k_n l_n e_n + \sum_{n=1}^{Nf_{i+}} k_n l_n e_n \right)}{\left( \sum_{n=1}^{Nf_{i-}} l_n e_n + \sum_{n=1}^{Nf_{i+}} l_n e_n \right)}$$

(A8)

867 The tensor components  $\bar{k}_i (i=1,2,3)$  in (A8) are an arithmetic mean of single-fracture  
868 permeability values weighted by open fracture surface areas at the sides of the whole  
869 fractured block. If we assume that these mean values are equal, irrespective of the facet of the  
870 fractured block (which also can go with fractured systems candidates to homogenization), it  
871 also means that the eventual anisotropy of permeability in the fracture network is just the  
872 consequence of fractures densities normal to the flow directions, i.e.,  $k_i^{FN-S} = \phi_i^{FN-S} \bar{k}$ .  
873 Notably, this strong assumption stating that one can define a constant single-fracture

874 permeability value  $\bar{k}$  also goes with the existence of an equivalent uniform single-fracture  
 875 aperture  $e_f$  for the whole fracture network. Reintroducing in (A5) the expression (A8) with a  
 876 constant value  $\bar{k}$  and making use of rescaled porosities defined in (A6) as  $\phi_i^{FN-S} = e_f \phi_i^{FN-S^*}$   
 877 comes down to

$$878 \quad s_i \approx \frac{e_f \bar{k} \sum_{j=1}^3 (-1)^{\delta_{i,j}} \phi_j^{FN-S^*}}{(\phi^{FN^*} - \phi_i^{FN-S^*}) \sum_{j=1}^3 (-1)^{\delta_{i,j}} k_j^f} \quad (A9)$$

879 It can also be shown that a WR network with constant aperture  $e_f$  for its three fracture  
 880 families has block and side porosities following the relation  $\sum_i \phi_i^{WR-S^*} = 2\phi^{WR^*}$ . If the rescaled  
 881 DFN is equivalent to the WR network, then one can state that  $\sum_i \phi_i^{FN-S^*} = 2\phi^{FN^*}$ . Noting that

$$882 \quad \sum_{j=1}^3 (-1)^{\delta_{i,j}} \phi_j^{FN-S^*} \text{ can also be rewritten as } \sum_{j=1}^3 \phi_j^{FN-S^*} - 2\phi_i^{FN-S^*} \text{ and reintroducing the preceding}$$

883 relationship between block and side porosities in (A9) results in

$$884 \quad s_i \approx \frac{2e_f \bar{k}}{\sum_{j=1}^3 (-1)^{\delta_{i,j}} k_j^f} \quad (A10)$$

885 In the case of field applications with poorly known and hardly accessible fracture  
 886 networks, (A10) returns the mean matrix block sizes in a fracture network based on the field  
 887 evaluations of the permeability tensor  $\mathbf{k}^f$  of a whole fractured block, the average uniform  
 888 aperture  $e_f$  and permeability  $\bar{k}$  of a single fracture. Because the entries of (A10) are not  
 889 straightforward to obtain and may also be associated with important measurement errors, it is  
 890 expected that (A10) will only render orders of magnitude of mean matrix block sizes.

891

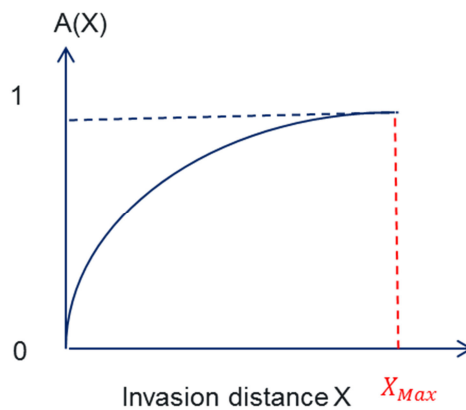
892 **Appendix B. Structural-geometrical evaluations of a mean matrix block size in a dual**  
893 **continuum flow model**

894 *The geometrical imbibition (GI) method*

895 The method has been developed for two-dimensional flow models only. Three-  
896 dimensional approaches are therefore handled as multilayer systems. For a two-dimensional  
897 image of an actual or synthetic fracture network, the first task to handle consists in mapping  
898 the image on a regular grid of square pixels. Each pixel is then assigned a value  $d_f$  that  
899 represents the distance between the center of the pixel and the closest fracture of the network.  
900 One sums up the area of pixels whose distance  $d_f$  is less than a prescribed value  $X$ , and the  
901 area is then normalized by the total surface area of the image to form the quantity  $A(X)$ . The  
902 resulting measure  $A(X)$  (Fig. B1) is modeled as

903 
$$A(X) = \frac{2X}{a} + \frac{2X}{b} - \frac{4X^2}{ab} \quad (\text{B1})$$

904 with  $a$  and  $b$  the resulting mean size of the matrix block of a two-dimensional dual porosity  
905 model.  $a$  and  $b$  are obtained by minimizing the sum of squared errors between the model in  
906 (B1) and the actual measures of  $A(X)$ .



907 Fig. B1. General imbibition technique to mean matrix block size identification. Normalized invaded  
908 matrix area  $A(X)$  as a function of the distance  $X$  between a location in the matrix and the closest  
909 fracture.  
910

911

912 ***The extended geometrical imbibition (EGI) method***

913 This method improves the two-dimensional GI technique by assuming that two mean  
 914 matrix block sizes characterize the relationships between fractures and matrix. For locations  
 915 in the matrix close to fractures, two types of matrix block interact with fractures, whereas  
 916 locations far from fractures are influenced by a single size of matrix block. This feature makes  
 917 that the quantity  $A(X)$  drawn from the mapping of the actual fracture network (see above the  
 918 GI technique) is modeled by a discontinuous curve in the form

$$919 \quad A(X) = \alpha_1 \left( \frac{2X}{a_1} + \frac{2X}{b_1} - \frac{4X^2}{a_1 b_1} \right) + \alpha_2 \left( \frac{2X}{a_2} + \frac{2X}{b_2} - \frac{4X^2}{a_2 b_2} \right) ; X \leq \frac{a_1}{2} \quad (B2)$$

$$A(X) = \alpha_2 \left( \frac{2X}{a_2} + \frac{2X}{b_2} - \frac{4X^2}{a_2 b_2} \right) ; X > \frac{a_1}{2}$$

920 with  $(a_1, b_1)$ ,  $(a_2, b_2)$  the size of the small and large matrix blocks respectively.  $\alpha_1, \alpha_2$  are the  
 921 proportions of small (type 1) blocks and large (type 2) blocks with  $\alpha_2 = 1 - \alpha_1$ . The distance  
 922  $X = a_1/2$  is the threshold beyond which a single type of large matrix block is sufficient to  
 923 model interactions between fractures and matrix.

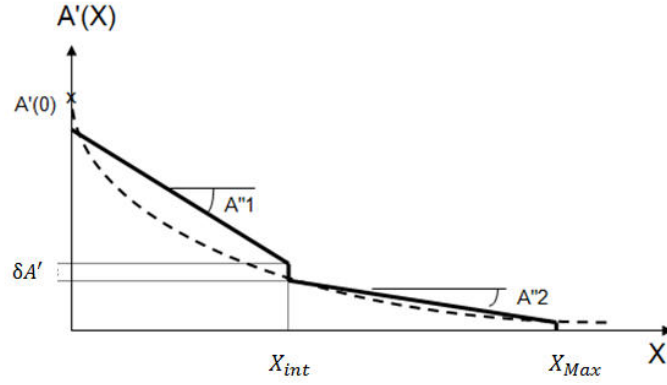
924 The inference of a single set of parameters  $(\alpha_1, a_1, b_1, \alpha_2, a_2, b_2)$  by minimizing errors  
 925 between the model in (B2) and actual measures of  $A(X)$  is not straightforward because the  
 926 subsets of parameters  $(\alpha_1, a_1, b_1)$  and  $(\alpha_2, a_2, b_2)$  are partly interchangeable to shape the same  
 927 function  $A(X)$ . It is better suited to analyze the derivative  $A'(X)$

$$928 \quad A'(X) = \frac{dA(X)}{dX} = \alpha_1 \left( \frac{2}{a_1} + \frac{2}{b_1} - \frac{8X}{a_1 b_1} \right) + \alpha_2 \left( \frac{2}{a_2} + \frac{2}{b_2} - \frac{8X}{a_2 b_2} \right) ; X \leq \frac{a_1}{2} \quad (B3)$$

$$A'(X) = \frac{dA(X)}{dX} = \alpha_2 \left( \frac{2}{a_2} + \frac{2}{b_2} - \frac{8X}{a_2 b_2} \right) ; X > \frac{a_1}{2}$$

929 This derivative appears as a decreasing piece-wise linear function of  $X$  which can be fitted by  
 930 hand or numerically on the plot of actual values  $A'(X)$  (see Fig B2). The parameter  $a_1$  is set

931 so that the break point of the model  $A'(X)$  located in  $a_1/2$  matches with the change of slope  
 932 of actual data. The parameter  $a_2$  is defined as the length (distance) for which  $A'(a_2/2) = 0$   
 933 (see Fig. B2).



934  
 935 Fig. B2. Enhanced general imbibition technique to mean matrix block size evaluation. First-order  
 936 derivative of the normalized invaded matrix area  $A(X)$  as a function of the distance  $X$  between a  
 937 location in the matrix and the closest fracture. The derivative with respect to  $X$  is modelled as a piece-  
 938 wise linear function allowing to infer a small and a large matrix block size.

939

940 The threshold  $a_1/2$  separates the linear function  $A'(X)$  in two portions with slopes

$$941 \quad A''_1 = \frac{dA'(X)}{dX} = -\frac{8\alpha_1}{a_1 b_1} - \frac{8\alpha_2}{a_2 b_2} ; X \leq \frac{a_1}{2} \quad (B4)$$

$$942 \quad A''_2 = \frac{dA'(X)}{dX} = -\frac{8\alpha_2}{a_2 b_2} ; X > \frac{a_1}{2}$$

942 The difference of slopes on a plot of  $A'(X)$  can be identified with the expression of  
 943  $A''_1 - A''_2 = -8\alpha_1/a_1 b_1$  which in turn fixes the ratio  $\alpha_1/b_1$  since  $a_1$  has been previously  
 944 prescribed.

945 The height of the step between the two linear portions of  $A'(X)$  can be calculated as

$$946 \quad \delta A' = A'\left(\left(\frac{a_1}{2}\right)^-\right) - A'\left(\left(\frac{a_1}{2}\right)^+\right) = \frac{2}{\alpha_1} \left( \frac{1}{a_1} - \frac{1}{b_1} \right) \quad (B5)$$

947 Identifying (B5) with the value of the plot and associating the result with the identified value  
 948  $A''_1(X) - A''_2(X)$  renders two equations allowing for the calculation of both  $\alpha_1$  and  $b_1$   
 949 values.

950 Finally, the expression of  $A'(X)$  in  $X = 0$  which writes as

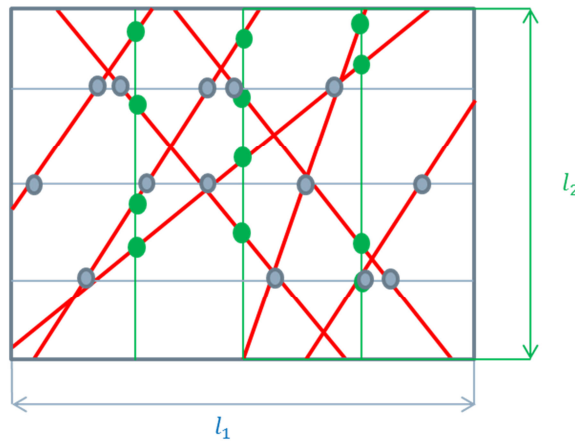
$$951 \quad A'(0) = \alpha_1 \left( \frac{2}{a_1} + \frac{2}{b_1} \right) + (1 - \alpha_1) \left( \frac{2}{a_2} + \frac{2}{b_2} \right) \quad (B6)$$

952 is identified via the equivalent value observed on the plot of actual data (Fig. B2) and returns  
 953 the value of  $b_2$ .

954

955 ***The mean spacing (MS) technique***

956 The principle of MS is sketched in Fig. B3.



957

958 Fig. B3. Mean spacing technique to mean matrix block size evaluation. Distances between neighbor fractures are  
 959 measured via the intersections between the fracture network and random lines parallel to the main directions of  
 960 the fractured block.

961 For each main direction  $i$  of a fractured block with length  $l_i$ , random lines parallel to  
 962 direction  $i$  and crossing the whole block are drawn. For each line, one counts as  $n_i$  the  
 963 number of intersections between the line and any fracture plane (or trace in a two-dimensional  
 964 problem) of the fracture network. For each random line in the direction  $i$ , the mean distance



965 between two successive intersections is  $l_i/(n_i + 1)$ . The mean size of the matrix block in the  
966 direction  $i$  is defined as

$$967 \quad s_i = l_i \left\langle \frac{1}{n_i + 1} \right\rangle \quad (\text{B7})$$

968 where averaging  $\langle \rangle$  is conducted over the whole set of random lines in the direction  $i$ .

969

970 **References**

971 Adler, P.M., Mourzenko, V.V., Thovert, J-F., Bogdanov, I., 2005. Study of single and  
972 multiphase flow in fractured porous media, using a percolation approach, *Dynamics of Fluids*  
973 *and Transport in Fractured Rocks*, Geoph. Monog. Series, 162, 33-41.

974

975 Acuna, J.A., Yortsos, Y.C., 1995. Application of fractal geometry to the study of networks of  
976 fractures and their pressure transient. *Water Resour. Res.* 31(3), 527-540.

977

978 Arbogast, T., 1990. Derivation of the double-porosity model of single-phase flow via  
979 homogenization theory. *SIAM J. Math. Anal.* 21, 823-836.

980

981 Barenblatt, G., Zheltov, I., Kochina, I., 1960. Basic concepts in the theory of seepage of  
982 homogeneous liquids in fissured rocks. *J. Appl. Math.* 24, 1286-1303.

983

984 Bourbiaux, B., Cacas, M., Sarda, S., Sabathier, J., 1997. A fast and efficient methodology to  
985 convert fractured reservoir images into a dual-porosity model. SPE-38907-MS.

986

987 Bourbiaux, B., Fourno, A., Delaplace, P., 2006. Method of modelling a porous geological  
988 environment through which a network of fractures run. Patent 2,009,098,366.

989

990 Bourbiaux, B., 2010. Fractured reservoir simulation: a challenging and rewarding issue. *Oil*  
991 *Gas Sci. Technol.* 65, 227-238.

992

993 Brooks, R.H., Corey, A.T., 1964. Hydraulic properties of porous media: *Hydrology papers*,  
994 Colorado State University. 3.

995

996 Coats, K.H., 1989. Implicit compositional simulation of single-porosity and dual porosity  
997 reservoirs. SPE -18427-MS.

998

999 De Dreuzy, J. R., Rapaport, A., Babey, T., Harmand, J. , 2013. Influence of porosity  
1000 structures on mixing-induced reactivity at chemical equilibrium in mobile/immobile Multi-  
1001 Rate Mass Transfer (MRMT) and Multiple INteracting Continua (MINC) models. Water  
1002 Resour. Res. 49(12), 8511-8530.

1003

1004 Folch, R., Casademunt, J., Hernandez-Machado, A., Ramirez-Piscina, L., 1999. Phase-Field  
1005 model for Hele Shaw flows in arbitrary viscosity contrasts. I- Theoretical approach. Phys.  
1006 Rev. E 60(2), 1724-1733.

1007

1008 Fournon, A, Grenier, C., Benabderrahmane, H., Delay, F., 2013. A continuum voxel approach  
1009 to model flow in 3D fault networks: A new way to obtain up-scaled hydraulic conductivity  
1010 tensors of grid cells. J. Hydrol. 493, 68-80.

1011

1012 Jourdain, X., Colliat, J.B., De Sa, C., Benboudjema, F., Gatuingt, F., 2014. Upscaling  
1013 permeability for fractured concrete: meso–macro numerical approach coupled to strong  
1014 discontinuities. Int. J. Numer. Anal. Met. 38(5), 536-550.

1015

1016 Karimi-Fard, M., Gong, B., Durlofsky, L.J., 2006. Generation of coarse-scale continuous flow  
1017 models from detailed fracture characterization. Water Resour. Res. 42, W10423.

1018

1019 Kazemi, H., Merrill, L.S., Porterfield, K.L., Zeman, P.R., 1976. Numerical simulation of  
1020 water-oil flow in naturally fractured reservoirs. *SPE Reserv. Eval. Eng.* 11(4), 750-758.  
1021

1022 Landereau, P., Noetinger, B., Quintard, M., 2001. Quasi-steady two-equation models for  
1023 diffusive transport in fractured porous media large-scale properties for densely fractured  
1024 systems. *Adv. Water Resour.* 24(8), 863-876.  
1025

1026 Lemonnier, P., Bourbiaux, B., 2010a. Simulation of naturally fractured reservoirs. State of the  
1027 art, part 1, Physical mechanisms and simulator formulation. *Oil Gas Sci. Technol.* 65(2), 239-  
1028 262.  
1029

1030 Lemonnier, P., Bourbiaux, B., 2010b. Simulation of naturally fractured reservoirs. State of the  
1031 art, part 2, Matrix-fracture transfers and typical features of numerical studies. *Oil Gas Sci.*  
1032 *Technol.* 65(2), 263-286.  
1033

1034 Lim, K.T., Aziz, K., 1995. Matrix-fracture transfer shape factors for dual porosity simulators.  
1035 *J. Petrol. Sci. Eng.* 13, 169-178.  
1036

1037 Long, J.C.S., Remer, J.S., Wilson, C.R., Witherspoon, P.A., 1982. Porous medium equivalent  
1038 for networks of discontinuous fractures. *Water Resour. Res.* 18(13), 645-658.  
1039

1040 Matthai, S.K., Nick, H.M., 2009. Upscaling two-phase flow in naturally fractured reservoirs.  
1041 *The AAPG Bull.* 93(11), 1621-1632.  
1042

1043 Narr, W., 1996. Estimating average fracture spacing in subsurface rock. The AAPG Bull.  
1044 80(10), 1565-1586.  
1045

1046 Neuman, S.P., 1988. A proposed conceptual framework and methodology for investigating  
1047 flow and transport in Swedish crystalline rock. SKB Swedish Nuclear Fuel and Waste  
1048 Management Co., Stockholm, September, Arbetsrapport.  
1049

1050 Noetinger, B., Estébenet, T., 2000. Up-scaling double porosity fractured media using  
1051 continuous-time random walks method. Transport Porous Med. 39(13), 315-337.  
1052

1053 Noetinger B., Estebenet, T., Landereau, P., 2001. A direct determination of the transient  
1054 exchange term of fractured media using a continuous time random walk method. Transport  
1055 Porous Med. 44, 539-557.  
1056

1057 Noetinger, B., Jarrige, N., 2012. A quasi steady state method for solving transient Darcy flow  
1058 in complex 3D fractured networks. J. Comput. Phys. 231, 23-38.  
1059

1060 Oda, M., 1985. Geologic analysis of naturally fractured reservoirs. Geotechnique. 35, 483-  
1061 495.  
1062

1063 Park, C.M., Homsy, G.M., 1984. Two-phase displacement in Hele Shaw cells. Theory. J.  
1064 Fluid Mech. 139, 291-398.  
1065

1066 Pruess, K., Narasimhan, T.N., 1985. A practical method for modeling fluid and heat flow in  
1067 fractured porous media. SPE J. 25(1), 14-26.

1068

1069 Pruess, K. Wang, J.S.Y., Tsang, Y.W., 1990. On thermohydrologic conditions near high-level  
1070 nuclear wastes emplaced in partially saturated fractured tuff. 2- Effective continuum  
1071 approximation. *Water Resour. Res.* 26(6), 1249-1261.

1072

1073 Quintard, M., Whitaker, S., 1993. One and two-equation models for transient diffusion  
1074 processes in two-phase systems. *Adv. Heat Transf.* 23, 369-465.

1075

1076 Quintard, M., Whitaker, S., 1996. Transport in chemically and mechanically heterogeneous  
1077 porous media. *Adv. Water Resour.* 19, 29-60.

1078

1079 Tatomir, A.B., Szykiewicz, A., Class, H., Helming, R., 2011. Modeling two phase flow in  
1080 large scale fractured porous media with an extended multiple interacting continua. *CMES*  
1081 77(2), 81-112.

1082

1083 Thomas, L.K., Dixon, T.N., Pierson, R.G., 1983. Fractured reservoir simulation. *SPE J.*  
1084 23(11), 42-54.

1085

1086 Ueda, Y., Murata, S., Watanabe, Y., Funats, K., 1989. Investigation of the shape factor used  
1087 in the dual-porosity reservoir simulator. *SPE-19469-MS.*

1088

1089 Unsal, E., Matthäi, S.K., Blunt, M.J., 2010. Simulation of multiphase flow in fractured  
1090 reservoirs using a fracture-only model with transfer functions. *Comput. Geosci.* 14, 527-538.

1091

1092 Warren, J.E., Root, P.J., 1963. The behavior of naturally fractured reservoirs. SPE J. 3, 245-  
1093 255.